AD-A071 333 MISSION RESEARCH CORP SANTA BARBARA CALIF F/G 4/1
MEASUREMENT OF ELECTRON ATTACHMENT AND MOBILITY IN DRY AND WET --ETC(U)
DEC 78 M L PRICE, V A VAN LINT DNA001-78-C-0141

UNCLASSIFIED MRC/SD-R-31 DNA-4788T NL

1 OF 1
AD A071333

END
DATE FILMED
8-79
DDC

DNA 4788T

MEASUREMENT OF ELECTRON ATTACHMENT AND MOBILITY IN DRY AND WET AIR

Mission Research Corporation
P.O. Drawer 719
Santa Barbara, California 93102

December 1978

Topical Report for Period July 1978—December 1978

CONTRACT No. DNA 001-78-C-0141

APPROVED FOR PUBLIC RELEASE;
DISTRIBUTION UNLIMITED.

THIS WORK SPONSORED BY THE DEFENSE NUCLEAR AGENCY
UNDER RDT&E RMSS CODE B323078464 R99QAXEA09182 H2590D.

Prepared for

Director
DEFENSE NUCLEAR AGENCY
Washington, D. C. 20305

Destroy this report when it is no longer needed. Do not return to sender.

PLEASE NOTIFY THE DEFENSE NUCLEAR AGENCY, ATTN: TISI, WASHINGTON, D.C. 20305, IF YOUR ADDRESS IS INCORRECT, IF YOU WISH TO BE DELETED FROM THE DISTRIBUTION LIST, OR IF THE ADDRESSEE IS NO LONGER EMPLOYED BY YOUR ORGANIZATION.

UNCLASSIFIED

SECURITY CLASSIFICATION OF THIS PAGE *(When Data Entered)*

REPORT DOCUMENTATION PAGE		READ INSTRUCTIONS BEFORE COMPLETING FORM
1. REPORT NUMBER DNA 4788T	2. GOVT ACCESSION NO.	3. RECIPIENT'S CATALOG NUMBER
4. TITLE *(and Subtitle)* MEASUREMENT OF ELECTRON ATTACHMENT AND MOBILITY IN DRY AND WET AIR		5. TYPE OF REPORT & PERIOD COVERED Topical Report for Period July 1978—December 1978 6. PERFORMING ORG. REPORT NUMBER MRC/SD-R-31
7. AUTHOR(s) Melvin L. Price Victor A. J. van Lint		8. CONTRACT OR GRANT NUMBER(s) DNA 001-78-C-0141
9. PERFORMING ORGANIZATION NAME AND ADDRESS Mission Research Corporation P.O. Drawer 719 Santa Barbara, California 93102		10. PROGRAM ELEMENT, PROJECT, TASK AREA & WORK UNIT NUMBERS Subtask R99QAXEA091-82
11. CONTROLLING OFFICE NAME AND ADDRESS Director Defense Nuclear Agency Washington, D.C. 20305		12. REPORT DATE December 1978 13. NUMBER OF PAGES 66
14. MONITORING AGENCY NAME & ADDRESS*(if different from Controlling Office)*		15. SECURITY CLASS *(of this report)* UNCLASSIFIED 15a. DECLASSIFICATION/DOWNGRADING SCHEDULE

16. DISTRIBUTION STATEMENT *(of this Report)*

DISTRIBUTION STATEMENT A
Approved for public release; Distribution Unlimited

17. DISTRIBUTION STATEMENT *(of the abstract entered in Block 20, if different from Report)*

Approved for public release; distribution unlimited.

18. SUPPLEMENTARY NOTES

This work sponsored by the Defense Nuclear Agency under RDT&E RMSS Code B323078464 R99QAXEA09182 H2590D.

19. KEY WORDS *(Continue on reverse side if necessary and identify by block number)*

Electron
Attachment
Mobility
Air

20. ABSTRACT *(Continue on reverse side if necessary and identify by block number)*

The experiments described in this report measured electron attachment and mobility in air as a function of electric field and water vapor partial pressure. The relevant rates were inferred from measurements of the current across a parallel plate ionization chamber to a short pulse of ionizing radiation.

DD FORM 1 JAN 73 1473 EDITION OF 1 NOV 65 IS OBSOLETE

UNCLASSIFIED

SECURITY CLASSIFICATION OF THIS PAGE *(When Data Entered)*

PREFACE

The mobility, μ, and attachment rate, α, in air are primary parameters in the calculation of the electromagnetic pulse generated by atmospheric nuclear explosions. These parameters determine the conductivity in ionized air, which limits the peak electric field generated by Compton recoil currents.

These parameters depend in a complex manner on the electric field (via the effect of electric field on average free-electron energy) and on the water vapor content of air (which also affects the electron energy distribution, decreases the mobility and participates as a third body in the attachment).

Previous experimental data have been reviewed by Longley and Longmire.[1] The only data that existed was the effectiveness of H_2O as a third-body with no E-field applied. For lack of a better model, they assumed that the third-body effectiveness of H_2O was constant relative to O_2 over the electron energy range. Using this assumption they constructed a model for predicting μ and α as a function of H_2O content and electric field. Some AURORA experiments were performed by HDL to check these values at realistic pressures and dose rates.[2] The results were somewhat scattered, but suggested that the effects of H_2O on μ and α had been overpredicted. The experiments reported herewith were conducted to resolve these uncertainties.

CONTENTS

SECTION 1

1.0 INTRODUCTION

The experiments described in this report measured electron attachment and mobility in air as a function of electric field and water vapor partial pressure. The relevant rates were inferred from measurements of the current across a parallel plate ionization chamber to a short pulse of ionizing radiation.

The electron density, n, in an air gas sample exposed to ionizing radiation obeys the relation:

$$\frac{dn}{dt} = K_g \dot{D} P - \alpha N$$

$$\alpha = K_{O_2\text{-}O_2} N_{O_2}^2 + K_{O_2\text{-}N_2} N_{O_2} N_{N_2} + K_{O_2\text{-}H_2O} N_{O_2} N_{H_2O} + K_{O_2} N_{O_2}$$

where K_g is the electron-ion generation per unit volume and dose at one atmosphere pressure in the gas mixture; $\dot{D}$ is the ionization dose rate in the gas; P is the gas pressure referred to standard temperature; N_{O2}, N_{N2}, and N_{H2O} are the respective molecular densities; $K_{O_2\text{-}O_2}$, $K_{O2\text{-}N_2}$, and $K_{O2\text{-}H_2O}$ are the rate constants for three body attachment of electrons to O_2 stabilized by O_2, N_2 or H_2O respectively; K_{O_2} is the two-body attachment coefficient for electrons to O_2 (at the higher electron energies). In the experiment the electron density was inferred from a measurement of the electron drift current across a parallel plate ionization chamber:

$$I = e_o A n \mu E ,$$

where A is the effective plate area, μ is the electron mobility, and E is the electric field. The rate of creation of electrons by the ionization pulse is deduced from the dose rate: $g = K_g \dot{D} P$, where $\dot{D}$ is the dose rate, P the pressure, and K_g is a constant dependent on gas composition.

The coefficients α and μ are a function of the gas composition and of the energy spectrum of the drifting electrons. The latter is determined by E/P and the gas composition (e.g., H_2O is much more effective in thermalizing electrons than N_2 or O_2).

At atmospheric pressure in air, $\alpha \sim 10^{-8}$ sec^{-1}. Therefore a significant fraction of the electrons are attached during a radiation pulse of duration $\sim$ 15 ns. At reduced pressure α can be decreased to the point that attachment during the pulse is negligible. In this case the mobility, μ, can be deduced from the peak current, I, and the electron density, which is inferred from the known dose, $D = \int \dot{D} dt$. The value of α can be inferred from the decay of the current after the ionization pulse. At atmospheric pressure we can infer μ/α from the the relation:

$$\int_0^\infty I dt = e_o A \mu E \int n dt = \frac{e_o A \mu E K_g P D}{\alpha} .$$

This relation is true for all values of α as long as the other terms are constants and there are no competing electron removal processes.

In practice this experiment has to avoid, or correct for, a number of interfering processes; including:

1) Electrons and ions may recombine at high ionization densities.

2) Electrons swept out of the ionized gas onto the anode no longer contribute current at later times.

3) The space-charge layers due to ions left near the cathode decrease the electric field where the electrons are moving.

4) The external circuit may decrease the bias voltage applied to the ion chamber while current is flowing.

5) Capacitive coupling of the output signal to the measuring instrument may distort it.

6) Net Compton electron currents to the sample plates interfere with the measurement of conduction currents.

In addition, the precision of the data depends on the following calibrations:

1) dose in the ionization pulse, D;

2) dose-to-ionization density conversion factor, K_g;

3) effective area of the ionization chamber, A;

4) pressure, P, and composition of the gas,

5) voltage applied to the chamber and plate spacing, which determine the applied electric field, E_o;

6) calibration of measuring resistor, which relates output voltage to current;

7) voltage calibration of measuring oscilloscope, and

8) time base calibration of measuring oscilloscope.

In Section 2 we will discuss the details of the experimental equipment and the data processing. The determination of relevant calibration factors will be discussed in Section 3, followed by the experimental results in Section 4. A summary of the data and conclusions will be presented in Section 5.

SECTION 2

2.0 EXPERIMENTAL DETAILS

2.1 Ionization Cell

The cell assembly used to contain the test gases during photon exposures is shown in Figure 2.1. Each of the three cells was designed to be a parallel plate ionization chamber with a center insulated electrode and two equidistant ground electrodes on either side. The body of the cylinder was constructed using aluminum plates and an aluminum thin-walled tube was used to maintain the correct separation between plates. In order to provide for vacuum conditions inside the test cell, an O-ring groove was machined in the tubing and a hermetically-sealed BNC connector was used to electrically couple to the center electrode. An aluminum tube was welded through the sidewall to provide a gas filling and vacuum port.

During all tests in which water vapor was part of the gas mixture used in the cell, a number of heating tapes were wrapped around the cell assembly to obtain and maintain temperatures well above the condensation point. Several thermisters placed at different locations on the cell assembly provided a measure of the temperature distribution.

2.2 HIFX

The photon generator used for these experiments was the High Intensity Flash X-Ray machine operated and maintained by HDL. It provides an

Cell	Gap (cm)
1	.536
2	.564
3	.523

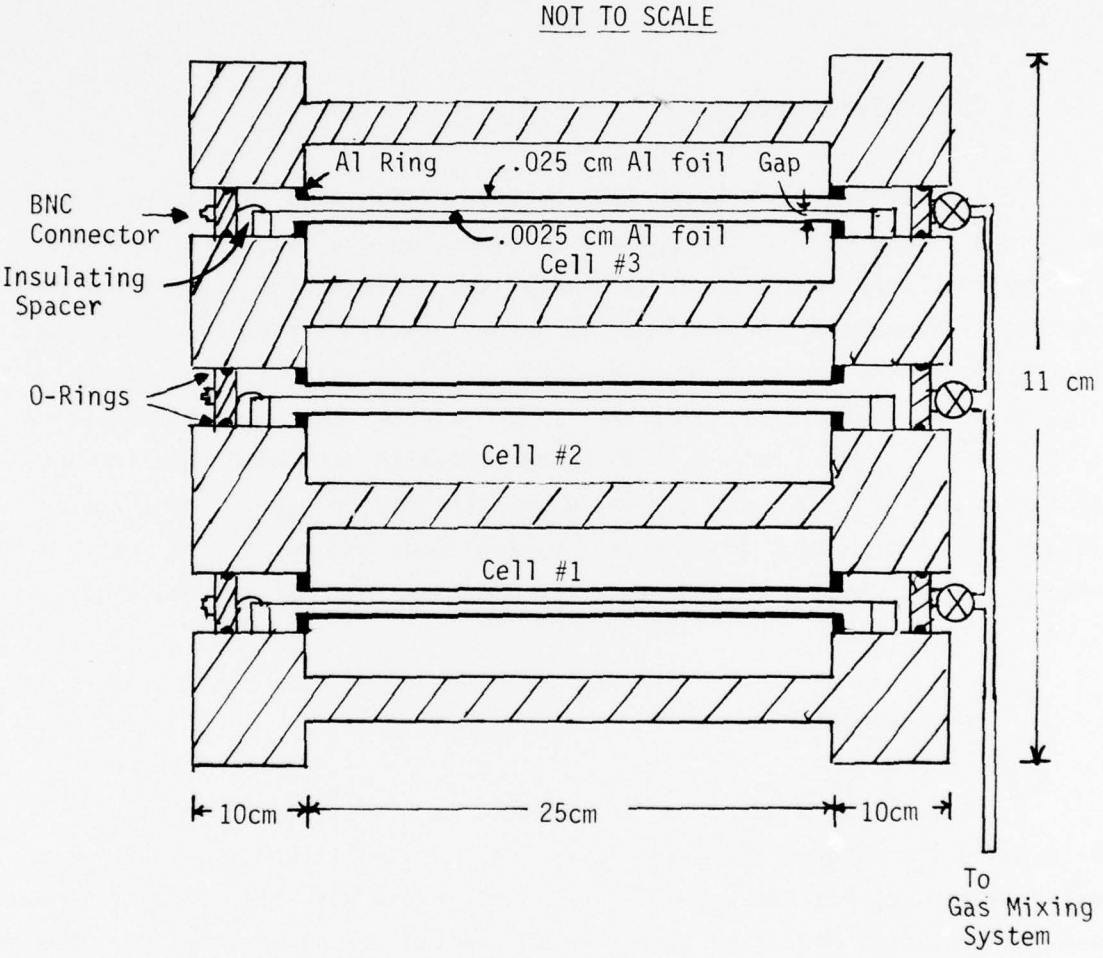

Figure 2.1. Ionization cell assembly used in HIFX Air Chemistry Experiments.

approximate 3 MeV Bremsstrahlung spectrum and for our tests was used in the "Crowbar" mode resulting in a pulse having FWHM $\cong$ 15 ns. During testing, several parameters were monitored by HDL to measure variations in the delivered radiation pulse; these were provided to us as a single oscilloscope photograph showing diode voltage and switch operation.

In addition, a scintillation/photodiode was operated by us during part of the experiment to observe the radiation pulse behind the ionization cell assembly.

2.3 Collimator Geometry

A specially constructed lead collimator was used during these tests. Two pieces of one cm aluminum plate were placed in the beam - one between the lead collimator and the cell assembly, the other at the rear of the cell assembly. The purpose of these plates was to provide a totally uniform environment around the test cells so that any scattered radiation passes through the same amount of shielding. The inside of the lead collimator was lined with 0.3 cm of aluminum to minimize radiation scattered from the lead entering the beam. Figure 2.2 shows a top view of the experimental configuration. The combination of thin center electrodes and collimated radiation reduced the net Compton current into the measuring circuit to negligible levels.

2.4 Measuring Circuit

All of the data to be discussed in this report were obtained while using the circuit shown in Figure 2.3. Noise, although troublesome in the beginning, was reduced to a level well below most of the experimental data. A few shots made with only 2 Volts applied across the test cell had a signal-to-background ratio around one but all of the other data had a ratio greater than ten when using the peak signal as a reference. Shielded data lines were brought out of the test area into the screen room and the signals displayed and photographed on Tektronix 150 MHz oscilloscopes. Separate high-voltage power supplies for each cell were used. The center cell alone

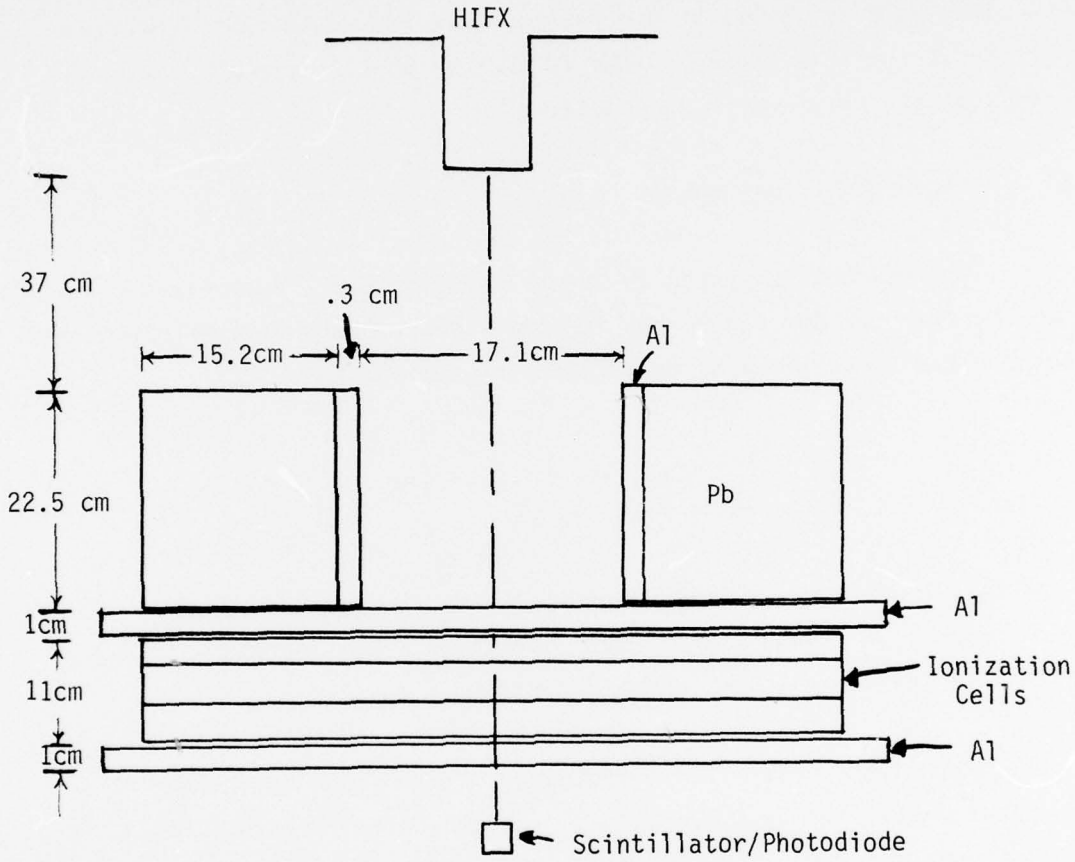

Figure 2.2. Top view of the HIFX experimental configuration.

used a power supply with both positive and negative isolated lines allowing us to place 100K resistors in the data circuit for additional isolation. Also, the center cell alone had the 10 MΩ monitor line brought into the screen room and measured on an ammeter.

2.5 Gas Handling and Measuring

The gas mixing system is shown in Figure 2.4. A premixed bottle of N_2 and O_2 (labeled dry air in the figure) was purchased from Matheson* who also provided a certificated measurement of the contents, viz.,

$$N_2 = 80.36\%,$$
$$O_2 = 19,64\%.$$

Helium, nitrogen and oxygen also purchased from Matheson were of research purity grade, i.e., less than 0.001% impurities. The SF_6 was provided by HDL and had less than 1.00% impurity content.

Water vapor came from a container of distilled water held at a temperature above 40° C. The partial pressure of water used to fill the test cell was measured, and was always well below the 40° C vapor pressure. Since the entire cell assembly and all connecting lines were maintained at 40° C, condensation was minimal.

Two other techniques were used to determine the amount of water in the test cell. First, a dew point measurement was used in which the gas mixture containing the water vapor was introduced into a glass cell constructed as shown in Figure 2.5. By carefully observing the mirrored surface while its temperature was reduced, it was sometimes possible to

---

* Matheson, 8800 Utica Avenue, Cucamonga, CA 91730.

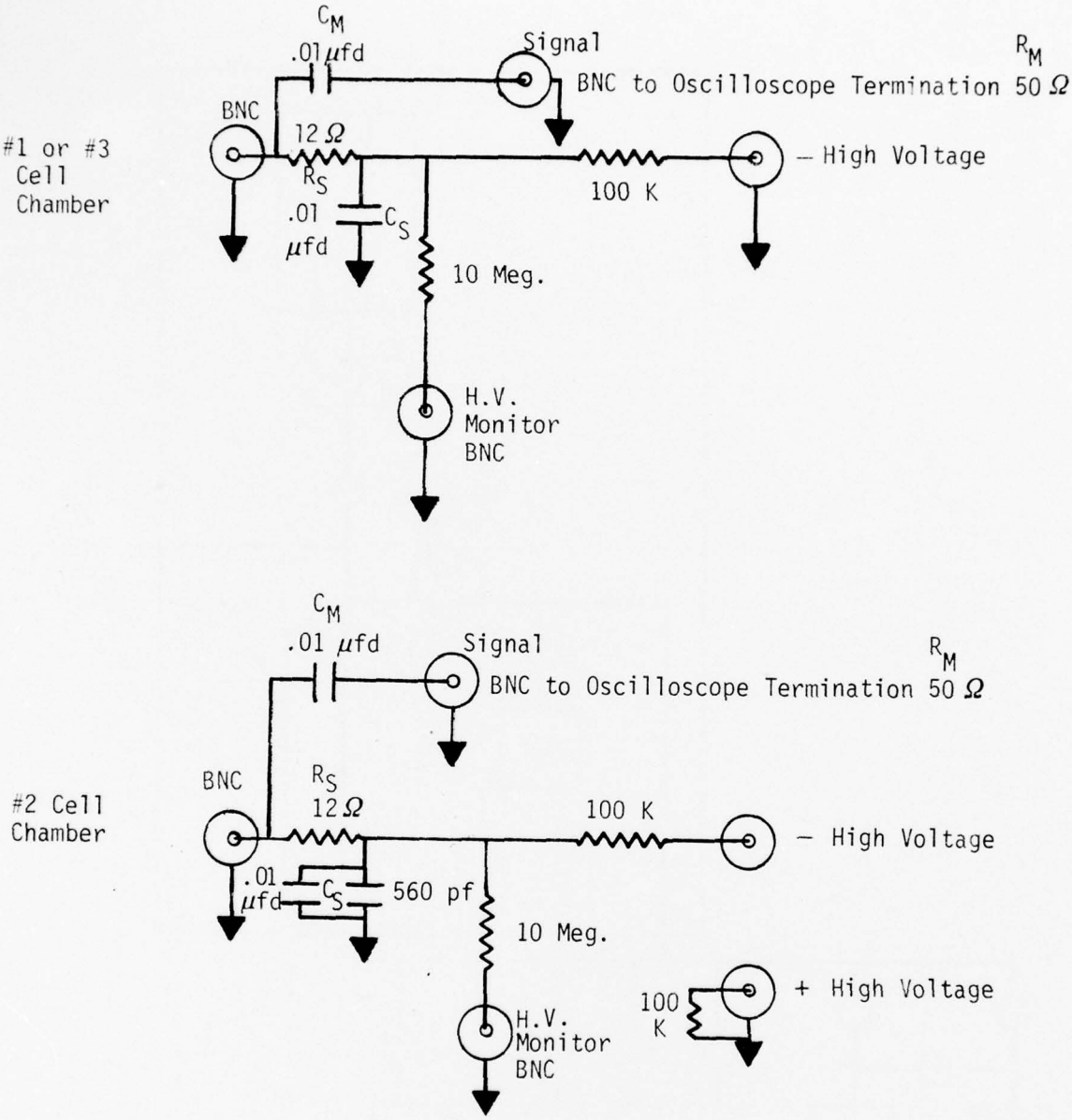

Figure 2.3. Termination, high voltage and data line circuit used during HIFX air chemistry experiments.

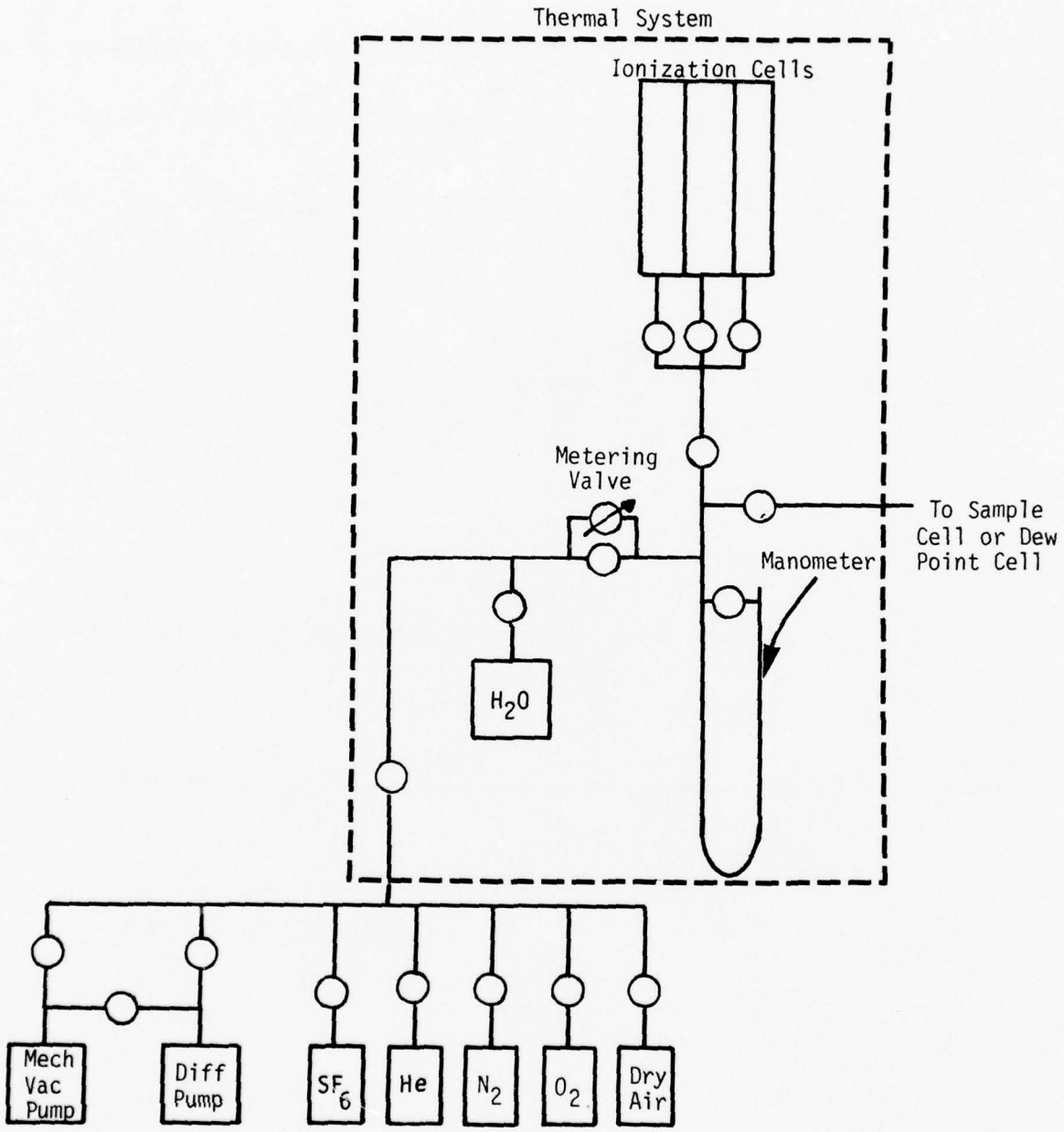

Figure 2.4. Gas mixing system for the HIFX air chemistry experiment. The Thermal System was used to maintain all components in contact with H_2O at or above +40° C.

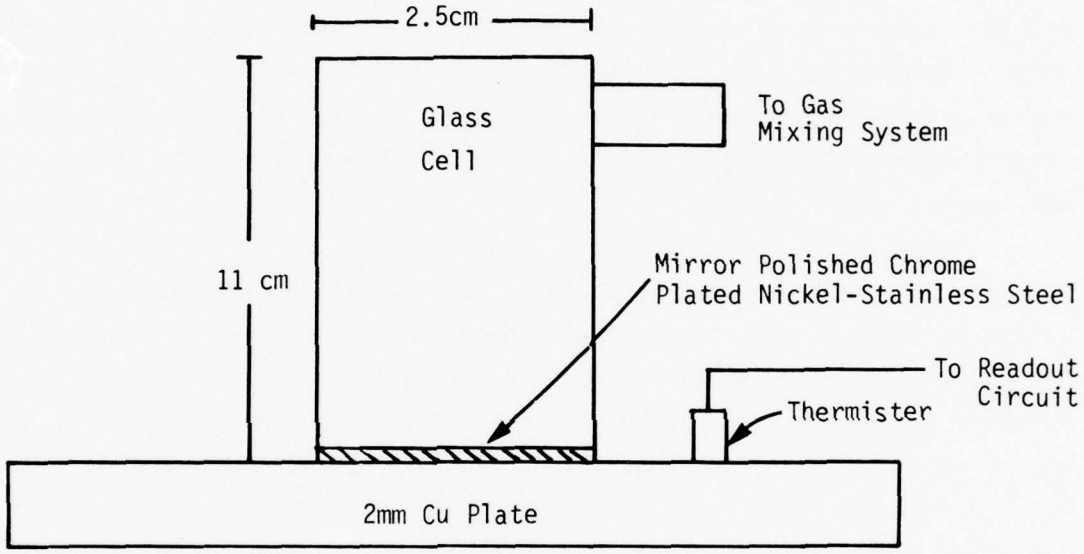

Figure 2.5. Apparatus used for dew point method of measuring water concentrations.

ascertain the onset of condensation. Then by noting the temperature and knowing the pressure, it was an easy exercise to look up the partial pressure of H_2O at that particular dew point and convert the results into a water concentration value. Unfortunately, the method was not always precise in that the onset of condensation occurred very slowly with a resulting spread in temperature over several degrees. Therefore we obtained useful data for only one of the gas mixtures. The other technique used to measure the amount of water in the gas sample consisted of obtaining a sample of the gas in a vacuum tight flask and having the contents analyzed by an independent laboratory using gas cromatography.* This was done for three gas samples.

A typical gas filling sequence begins with the evacuation of all lines and the test cell to a pressure below 1×10^{-3} Torr. For wet air shots, the vacuum pump valve would be shut and the water valve opened until the pressure inside the cell reached the desired value, as indicated on the manometer. Then the water valve was closed and the dry air cylinder valve opened until the desired final pressure was reached. At that time, the test cell valve was closed and the dry air flow stopped. A similar procedure was used to mix a 5% O_2 and 95% N_2 gas mixture during shots 142-145. All of the other shots used a single gas cylinder's contents and the cell filling consisted only of evacuating all of the lines and cell and then slowly filling the cell while reading the manometer (except for the helium cells as described in the next section.

2.6 Dose Measurement

The purpose of three ionization cells for each shot was to provide a dose calibration built into the experiment and not have to rely upon TLD or other external means to measure the dose. Also, since there was some

---

* Gollob Analytical Service Corporation, 47 Industrial Road, Berkeley Heights, NJ 07922.

attenuation of the beam due to the aluminum plates this loss could be deduced by comparing the front and rear cell's measured signals.

The outer cells were filled with a mixture of (~0.1 - 0.3%) N_2 and (99.7-99.9%) Helium. No attempt to accurately determine the N_2 was made but an estimated partial pressure of 1 Torr of N_2 mixed with He inside the cell. The purpose of this deliberate contamination of Helium was to insure that the energy required to produce one ion pair was 30 eV in agreement with the Penning Effect.[1] By measuring the total number of electrons produced in Helium, the dose could then be calculated.

During the test series, three different doses were used for different shots. They were produced by inserting additional shielding between the cell assembly and the beam. The three configurations are shown in Table 2.1. A photodiode was placed behind the cell assembly during shots 29-126. The record thus obtained gave a means to compare the shot-to-shot variation in pulse shape and amplitude.

Table 2.1. Shielding used to obtain different doses.

DOSE	SHIELDING*
High	None
Medium	10 cm Al
Low	10 cm Pb

* The aluminum plate placed between the collimator and the cell assembly remained for all shots. This table indicates additional shielding.

2.7 Data Processing

All of the data obtained during this experiment were on oscilloscope photographs showing voltage-time relations. Prior to analysis, these data were digitized and stored on cassettes using a Tektronix 4956 Graphics Tablet connected to a Tektronix 4051 computer terminal. Referring to Figure 2.3, before a value for the current produced in the ionization cell can be inferred from the oscilloscope photo, a correction must be applied to account for the effect of the circuit. This was done during analysis of the digitized data, again using the Tektronix 4051.

The current produced in the ionization cell, I(t), is related to the oscilloscope voltage, V(t), through the following equations.

$$I(t) = I_1(t) + I_2(t), \tag{2.1}$$

$$I_1(t) = \frac{1}{R_S} V_1(t) - \frac{1}{R_S C_S} \int_0^t V_1(\theta)\, e^{-(t-\theta)/R_S C_S}\, d\theta, \tag{2.2}$$

$$I_2(t) = V(t)/R_M , \tag{2.3}$$

$$V_1(t) = V(t) + \frac{1}{R_M C_M} \int_0^t V(\theta) d\theta. \tag{2.4}$$

Calibration measurements of the parameters R_M, C_M, R_S, and C_S were made and are discussed in Section 3 of this report.

Two additional corrections were applied to the data: one to account for sweep-out of the electrons; the other for the change in voltage due to the boundary layer near the cathode. The current generated by the ionization chamber is given by

$$I(t) - A\, e_o\, n\, \mu\, E\left(1 - \frac{X}{d}\right) , \tag{2.5}$$

where $$X = \int_0^t \mu E \, dt' \simeq \mu E t \ . \tag{2.6}$$

and d is the plate spacing. The attachment coefficient enters this equation through n, viz.,

$$n = n_o \exp(\alpha t), \tag{2.7}$$

where n_o is the total ionization-produced electron density. We define α', the measured logarithmic decay slope, by

$$\alpha' = - \frac{1}{I} \frac{dI}{dt} \ . \tag{2.8}$$

To first order in the correction terms:

$$\alpha' = \alpha + \frac{\mu E/d}{1-\mu E t/d} - \frac{1}{E} \frac{dE}{dt} \ ,$$

or $$\alpha = \alpha' - \frac{\mu E}{d} \left[1 - \frac{\mu E t}{d} \right]^{-1} + \frac{1}{E} \frac{dE}{dt} \tag{2.9}$$

which corrects the measured value, α', for sweep-out and the boundary layer voltage.

Boundary layer buildup, X_{BL}, results in a change in voltage ΔE, across the ionization cell. Equations defining these terms are

$$X_{BL} = \frac{\mu}{\alpha'} E_o, \tag{2.10}$$

and $$\Delta E = \frac{n_o X_{BL}^2}{2 E_o d^2} \ . \tag{2.11}$$

These are the approximate thicknesses of the boundary layer and the change in bulk electric field at the end of the attachment process. The effective electric field during attachment is somewhere between E_o and $E_o - \Delta E$.

For the data to be presented $\Delta E/E_o < .1$ and no corrections for the electric field changes by the boundary layers was applied. When sweep-out was important, α' was measured at the beginning of the decay only and the correction applied: $\alpha = \alpha' - \mu E/d$.

SECTION 3

3.0 CALIBRATIONS

3.1 Molecular Density Calculations

For all shots made during this experiment, the two outer cells contained the same gases and were both pressurized together. In all cases, they were filled with a mixture of (0.1-0.3)% N_2 and (99.7-99.9)% He. No attempt was made to accurately determine the N_2 but an estimated partial pressure of 1 Torr of N_2 mixed with He inside the cell to obtain the desired final pressure. The purpose of this deliberate contamination of He was to insure that the energy required to produce one ion pair was 30 eV in agreement with Penning ionization. Then by measuring the total number of electrons produced in He from a single radiation pulse, it was possible to calculate the dose (see next section).

Several different total pressures were used in the He cells for different shots. Table 3.1 lists all of the configurations during which useful data were obtained.

Cell #2 was used as the ionization chamber for several gas mixtures from which the electron mobility and attachment were measured. Table 3.2 shows all of the configurations used during HIFX testing. Of fundamental importance during these measurements was the exact molecular composition of the cell. Implicit in this statement is the requirement to simultaneously know the temperature and pressure for all of the gas species contained

Table 3.1. He cell (Cells 1 & 3) pressure used for various shots.

Shots	He Cells Total Pressure (atm)
30-34	1.0
35-65	0.5
66-76	0.4
77-83	0.1
84-148	0.4

Table 3.2. Gas mixtures contained in Cell #2 for different shots.

Shots	Total Pressure @293°K (atm)	Gas Mixture (Mole. Fraction)
30-38	.99	(1.0) O_2
39-40	.0993	(1.0) O_2
41-53	.25	(.804) N_2 - (.196) O_2
54-65	.99	(.804) N_2 - (.196) O_2
67-81	.50	(.804) N_2 - (.196) O_2
82-84	.99	(.804) N_2 - (.196) O_2
85-98	.47	(.043) H_2O - (.769) N_2 - (.188) O_2
99-116	.47	(.0229) H_2O - (.786) N_2 - (.192) O_2
117-126	.46	(.02) H_2O - (.788) N_2 - (.192) O_2
127-129	.42	(.055) H_2O - (.76) N_2 - (.185) O_2
130-140	.91	(.0275) H_2O - (.782) N_2 - (.153) O_2
142-145	.90	(.949) N_2 - (.051) O_2
146-148	.93	(1.0) SF_6

in the cell. Several different techniques and measurements were used to provide this information.

First, the gases obtained from Matheson were precisely specified. Many shots were made after filling Cell #2 with pure O_2, dry air, or SF_6. For these cases, the total pressure and temperature during filling were enough to deduce the gas density. This was accomplished using the mercury manometer and thermisters mounted on the cell assembly.

As indicated in Table 3.2, shots 142-145 were made while Cell #2 contained (.95) N_2 and (.05) O_2 gas mixture. These mole fractions were determined using partial pressure mixing of pure N_2 and O_2. Of course, the temperature was held constant during this mixing so the final density could be deduced.

The most difficult gas mixtures to specify were those in which water vapor was added to dry air to obtain the desired wet air composition. As described in Section 2.5, three different measurements were made of the water content. The results are shown in Table 3.3. All water mixing and testing of the mixture required that all components in contact with the H_2O be maintained at an elevated temperature in order to prevent condensation. A temperature of +40°C was used to accomplish this and provide an adequate margin above the dew point for the largest amount of water used. Several thermisters were mounted around the cell assembly to record the temperature held at or above +40° as was all tubing used to connect between the cell assembly and the gas mixing system.

There was concern over the possibility that sequential filling of gas would produce a non-uniform composition between the gas-filling network and the sample chamber. In particular, it would be easy for the filling system to be comparatively rich in the gas species added later.

Table 3.3. Water concentration results for different mixtures.

Sample	Shots	Water Concentration (Per cent)		
		Partial Pressure Measurement	Dew Point Measurement	Gas Chromatography Measurement
1	85-98	5.0	-	4.30
2	99-116	2.52	-	2.29
3	117-126	1.26	-	2.0
4	127-129	5.6	5.4	-
5	130-140	2.75	-	-

In these experiments we always added the species in order of increasing pressure. The volume of the gas-filling network was 3% of the volume of the sample chamber. Therefore, since no more than all of the gas species except the last can be expelled from the gas-filling network into the sample chamber, the fractional composition of all species except the last can be too large by no more than .001 %.

3.2 Dose Calculations

The quantity of primary interest is the number of electron-ion pairs per unit volume formed in the sample chamber times the area of the electron-ion cloud. The ion-pair density without the area also appears in small correction terms for the electric field. Since the photon beam is collimated to an area smaller than the effective area of the ion chamber electrodes, we expect the dose × area product to be almost constant in passing through the three ion chambers (except for very small attenuation in the Al walls and electrodes).

The variation of dose between photon pulses was measured with a scintillator-photodiode furnished by HDL and by the peak current in the helium-filled ion chambers. The standard deviation of the pulse heights was approximately 6%. For the present, no correction for individual pulse variations were applied.

The absolute ionization rates for the three intensities were deduced by five methods:

1) measurement of peak current in the He ion chambers, using an assumed drift mobility for electrons in He, and a ratio of ionization efficiencies in air relative to He;

2) measurement of the total charge collected in the He ion chambers and a ratio of ionization efficiencies in air relative to He,

3) measurement of peak current in 20:1 N_2:O_2 and an assumed mobility in N_2 (neglecting the effect of $< 5\%$ O_2 on mobility);

4) measurement of the dose in front and behind the ion chambers with thermoluminescent dosimeters (TLD's) and deducing the effective beam area from the geometry of the photon source, collimator and ion chambers; and

5) for the medium and low intensity configurations the dose was calculated from the high-intensity calibration by the ratio of scintillator-photodiode readings. In reducing the data the dose was converted for an effective beam area of 300 cm^2, the energy loss per ion pair in air was assumed to be 32.5 eV, and the energy loss per ion pair in N_2 contaminated He was assumed to be 30 eV.

The signals in the He ion chambers exhibited the effect of Penning ionization of impurities (presumably the .1% N_2 added purposely) as a short-term increase in current. Figure 3.1 illustrates this behavior. From the time scale ($\sim$50 ns) and the N_2 density ($\sim 1.5 \times 10^{16}$ cm^{-3}) we can estimate the cross section for ionizing N_2 by He metastables to be $\sim 10^{-14}$ cm^2, a reasonable value. Therefore, the signal shapes justify the use of the value of 30 eV per ion pair when applied to the extrapolated peak current.

At the same applied voltage the two ion chambers (front and rear) displayed the same current, within the accuracy of the measurement. The peak current in the He chambers was measured as a function of applied electric field. The results are plotted in Figure 3.2 for the three configurations: H (no shield), M (10 cm Al shield), and L (10 cm Pb shield). The fourth

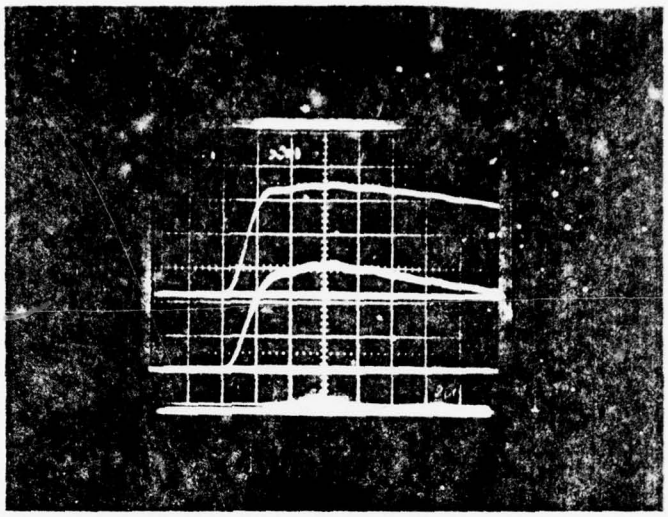

Figure 3.1. Signals from the two He ion chambers for Shot 95 showing the increase in current after the radiation pulse due to Penning ionization. Vertical scale is 40 mV/cm; horizontal scale is 20 ns/cm.

curve on Figure 3.2 is the published data on the drift velocity in He. The observed bias dependence agrees very well with this slope up to the onset of avalanche multiplication at high values of E_o/P.

Table 3.4 presents the results of these calibrations. The TLD readings exhibited a larger ratio of back-plane dose to average dose for the L configuration than for the H and M configurations, indicating that the more energetic radiation penetrating the 10 cm lead shield was less divergent than the unattenuated radiation. Therefore, the reading of the scintillator-photodiode (which was located at the back plane) was multiplied by an average/back-plane correction derived from the TLD data.

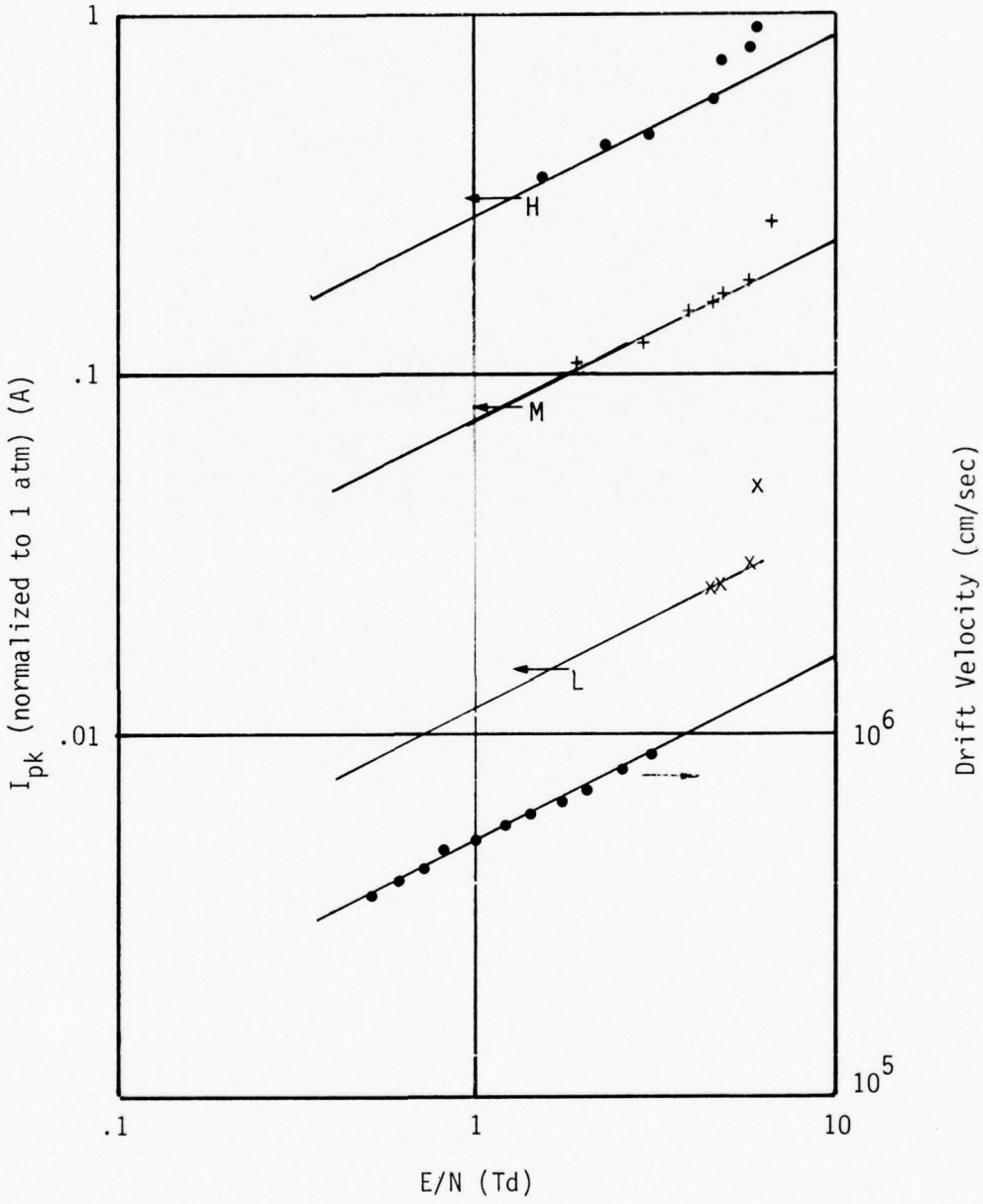

Figure 3.2. Bias dependence of He ion chamber current.

Table 3.4. Dose calibrations.

Dose Values in Rad(air)			
	CONFIGURATION		
METHOD	H	M	L
He Current	15.1	4.00	0.64
He Charge	14.7	3.45	0.52
N_2 Current	----	----	0.61
TLD	12.3	2.4	0.34
Scintillator Ratio	----	4.06	0.63*
Value Used	14.7	3.9	0.64

* Using a correction factor for the ratio of center-chamber dose to back-plane dose derived from TLD readings.

3.3 Physical Dimensions

The important dimensions are the ionization cell spacing and the radiation beam area as it moves through the cells. The former were measured prior to the experiments during cell assembly. Since the center electrode consisted of a sheet of .0025 cm Al foil, special care was required to obtain and maintain uniform spacing between plates. Measuring the gap at many points around the plate insured that this uniformity, in fact, was realized. Figure 2.1 shows the average value for each cell gap.

The beam area passing through the cells was defined by the collimator; Figure 2.2 shows the relevant dimensions. The cell assembly was placed on a wooden table in front of HIFX at a distance of 61.7 cm from the anode. Limiting the beam aperture at the collimator's exit to 17.5 cm insured that the beam spread while traveling through all three cells will be less than 4 cm for a total beam size less than 21.5 cm upon leaving the cell assembly. Referring to Figure 2.1, we see than a 25.4 cm window in the cells adequately contains the entire beam.

3.4 Circuit Parameters

As discussed in Section 2.7, exact values for the circuit elements were required in order to produce accurate values for the ionization current. These values were measured upon test completion using several different precision instruments.

The resistors were measured using a Wheatstone Bridge supplied by HDL. A capacitor bridge was used to measure values for the several circuit capacitors. Measured values are shown in Table 3.5.

Table 3.5. Measured values for the circuit elements.

Cell Number	R_M(Ohms)	C_M(μfd)	R_S(Ohms)	C_S(μfd)
1	50	.00845	13.14	.00991
2	50	.00926	12.54	.00996
3	50	.00867	12.13	.00767

A calibration of the voltage applied to the ionization cells was also conducted upon test completion. Cell #2 used a monitor line during the tests so that a measure of shot-to-shot variations could be obtained. Table 3.6 shows the results of the measurements along with the calculated values. All voltages were within 10% and except for 2, 5, and 2000 V were within 2%. Larger variations occurred in the current measurements due probably to resistance changes when subjected to voltages of 1 kV or greater.

The oscilloscopes used during the tests were calibrated both before and after the experiment. Time bases were compared with a standard generated by a Tektronix Type 180A Time Base Generator. No observable discrepancies were noted. Amplitude calibration of the various vertical amplifiers used in the oscilloscopes were made using the calibration pulse from a Tektronix Type 485 oscilloscope. To duplicate the experimental conditions, all of the data lines were included in this calibration. While making this calibration, one of the pre-amps for Cell #2 failed. After returning to San Diego, all of the data were examined and for many shots, both preamps for Cell #2 used the

Table 3.6. Results of measurements and calculations for the voltage applied to Cell #2.

APPLIED VOLTAGE	VOLTAGE			CURRENT (μA)		
	CALC	MEAS	CALC/ MEAS	CALC	MEAS	CALC/ MEAS
2	1.92	1.77	1.09	.19	.18	1.06
5	4.81	5.08	.94	.48	.49	.98
10	9.62	9.62	1.00	.96	.91	1.05
20	19.23	19.26	1.00	1.92	1.81	1.06
50	48.08	48.07	1.00	4.81	4.51	1.07
100	96.15	96.15	1.00	9.62	9.08	1.06
200	192.3	192.2	1.00	19.2	18.5	1.04
500	480.8	490.4	.98	48.1	47.7	1.01
1000	961.5	977.0	.98	96.2	105	.92
2000	1923.1	1750.0	1.10	192.3	237	.81

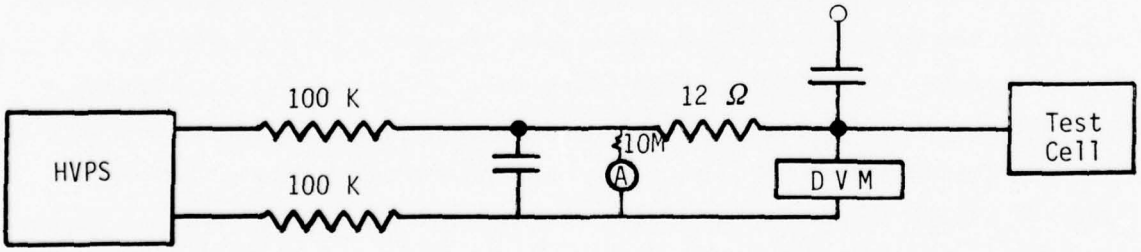

$$V_{Calc} = V_{Appl}\left[1 - \frac{2\times10^5}{5.2\times10^6}\right] = .962\ V_{Appl}$$

$$I_{Calc} = \frac{V_{Calc}}{10^7}$$

same gain settings. Thus a comparison of the signals allows for a check on the failed pre-amp. We conclude that it must have failed after the experiments were completed. No appreciable errors were moted and no corrections were applied to the data in this report as a result of oscilloscope calibrations.

3.5 Background Signals

Figure 3.3 illustrates the signal observed with no bias voltage on the sample chamber. This signal appeared to be independent of gas sample; it has the shape of the first derivative of the ionization pulse (apart from the small circuit oscillation after the pulse). The peak charge halfway in the pulse is $\sim 4\times10^{-11}$ coul.

A signal of this shape is expected from the space charge of Compton electrons moving through the sample chamber. An estimate of such a signal follows:

Dose rate $\approx 10^{9}$ rad/sec,

Compton current density $\approx (2\times10^{-12})\times10^{9} = 2\times10^{-3}$ A/cm^2,

Average longitudinal electron velocity $\approx 10^{10}$ cm/sec,

Space charge density $\approx 2\times10^{-13}$ C/cm^3, and

Charge induced in center electrode $\approx 2\times(2\times10^{-13})\times300$ cm^2 x (.5cm/2) $\approx 3\times10^{-11}$ Coul.

The agreement is well within the accuracy of the estimate.

The apparent net charge at late times in the record from Figure 3.3 is $\lesssim 10^{-9}$ Coul. This compares with net charge measured in 1 atm pure O_2 at only 5 V applied (E_o = 10 V/cm) of 1.4×10^{-8} Coul. Therefore, this background signal is negligible at all fields larger than 10 V/cm, particularly in air.

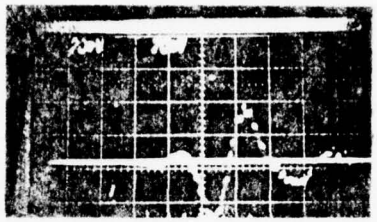

Figure 3.3. Signal observed on Cell #2 with zero Volts applied during Shot #30; gas was 1 atm pure O_2. Vertical scale is 20mV/cm; horizontal scale is 10 ns/cm.

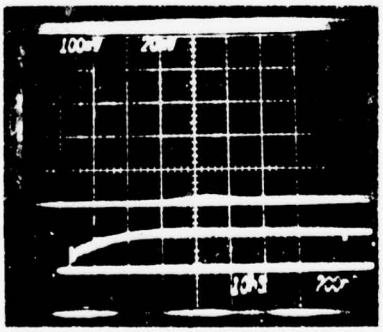

Figure 3.4. Signal observed on Cell #2 with 1000 V applied during Shot #147; gas was 1 atm SF_6. Vertical scale is 100 mV/cm for the top trace; 20 mV/cm for the bottom one; horizontal scale is 10 ns/cm.

The background was also checked with 1 atm of SF_6 in the chamber. Since SF_6 is a very rapidly attaching species, very little prompt signal is expected. At E_o = 20 V/cm the signal was essentially the same as the zero-volt signal discussed above. At E_o = 2000 V/cm the signal is shown in Figure 3.4. The prompt component is less than the prompt component in pure O_2 at the same field and pressure by a factor of 35. This is an upper limit to the possible interference by cable signals, conduction in external circuit wiring, etc. If this signal represents an electron current, it would correspond to a value of $\mu/\alpha \approx 3 \times 10^{-7}$.

The persistent delayed signal corresponds to a current from the ion chamber continually discharging the charge storage capacitor. The most likely cause is the current of positive and negative ions in the gas. The magnitude corresponds to an ion mobility (sum of positive and negative ion mobilities) of ~ 2 cm^2/V-sec, a reasonable value.

Therefore, the measured background signals represent known processes or make negligible contributions to the uncertainties in the reaction rates deduced from these experiments.

SECTION 4

4.0 RESULTS

We will discuss the results in three sections: pure O_2, dry air, and moist air. The O_2 experiments were performed first to check on the background without contaminating the gas handling system with SF_6. As it turns out the background appears to be so small that accurate data on O_2 were acquired. The dry air data were intended to compare with existing data in which the uncertainty was thought to be minimal. Finally, the moist air data represent the important new data.

4.1 O_2 Data

All O_2 measurements except one were made on a sample at 1 atm. Therefore, only (μ/α) can be deduced from the data. The results are plotted in Figure 4.1. The 0.1 atm data were scaled by $1/P^3$, assuming pure three body attachment. The data reported by Grünberg[3] are shown for comparison. Our values at $E_o/P \sim 100$ and 550 V/cm-atm are within 10% of Grünberg's, although our curve appears to dip more sharply at 170 V/cm-atm. At worst, a systematic increase of our values of (μ/α) by 20% would improve the overall agreement. This correction would correspond to our overestimating the carrier generation rate by 20%, i.e., assuming the actual dose in the H configuration is closer to the value measured with the TLD's than with the He ion chambers.

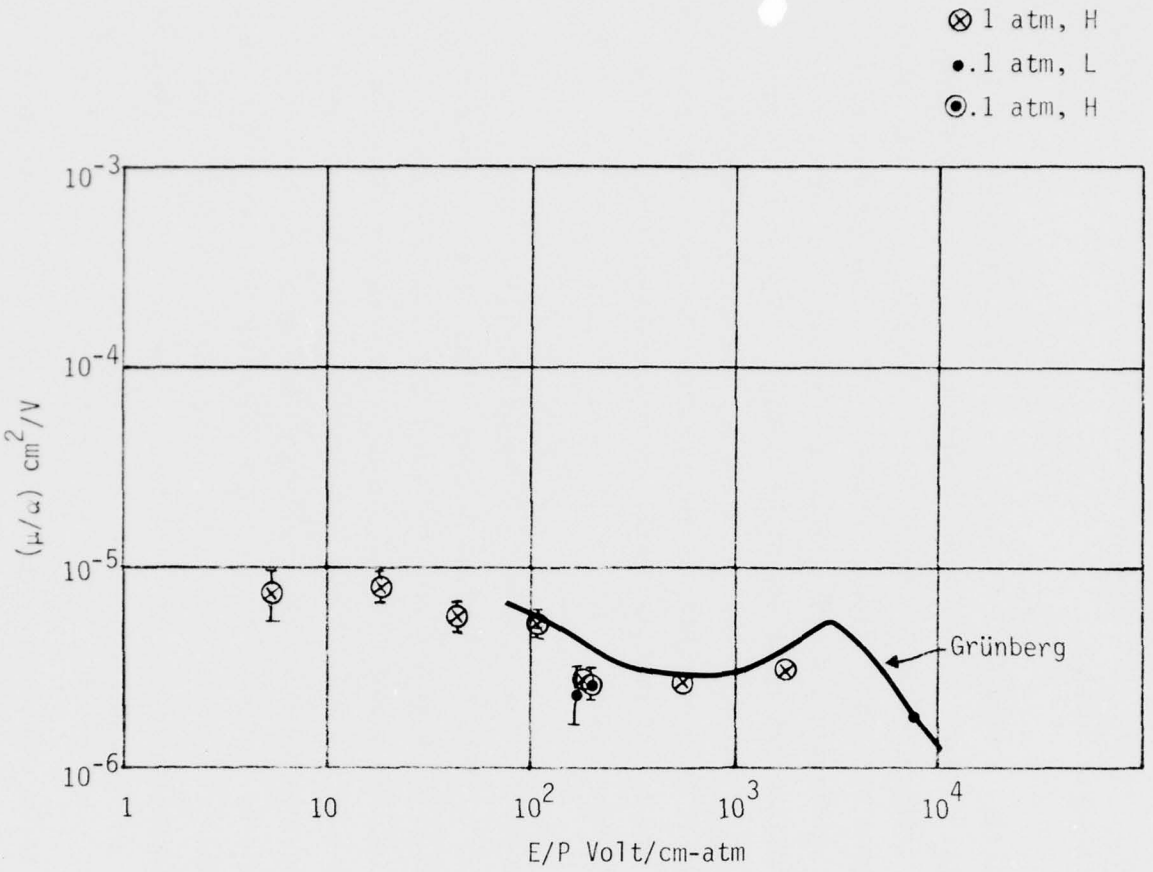

Figure 4.1. μ/α in pure O_2 (scaled to pure O_2).

4.2 Dry Air Data

Experiments were performed on dry air at 0.25, 0.5 and 1 atm and on a 20:1 N_2:O_2 mixture at 0.9 atm. In air at 1 atm the attachment coefficient was sufficiently high at all but the highest fields that only (μ/α) could be determined. At all other pressures α was measured from the current decay and μ from the peak current.

The mobility, scaled to 1 atm by 1/P, is shown in Figure 4.2 and is compared to Wyatt's[4] data. The shape of our data is more concave downward. Again the agreement would be improved by increasing our values of μ by 20%, in accordance with the TLD calibrations. This would produce excellent agreement at intermediate fields ($E/P \sim 10^2$ V/cm-atm) but still significantly lower mobilities at lower and higher fields. The two data for 20:1 N_2:O_2 are in excellent agreement with the dry air data, as expected since N_2 is the principal scattering center in both cases. The excellent agreement between the H, M, and L configuration data demonstrates that the ratio of doses was correctly evaluated.

The attachment rates, scaled to 1 atm of dry air according to P^2 (assuming three body attachment only), are shown in Figure 4.3. The curve is deduced by Longley and Longmire[1] from the low pressure drift-tube data of Phelps. Our data exhibit a surprising discrepancy between the values of α deduced from the 0.25 atm and 0.5 atm measurements at low E/P. In this regime the attachment is known to be exclusively three-body, so that the scaling by P^2 should be correct. A possible explanation is that at 0.5 atm the electrons do not have time to lose the energy acquired in the ionization event prior to attachment.* Note that these data depend only on the shape of the current decay, not on the dose calibration.

We will focus attention on the .5 and 1 atm data, because these are less affected by sweep-out and boundary layer corrections. It appears clear that the dip in α at higher fields just before the onset of two body

---

* We are indebted to Bill Crevier for this suggestion.

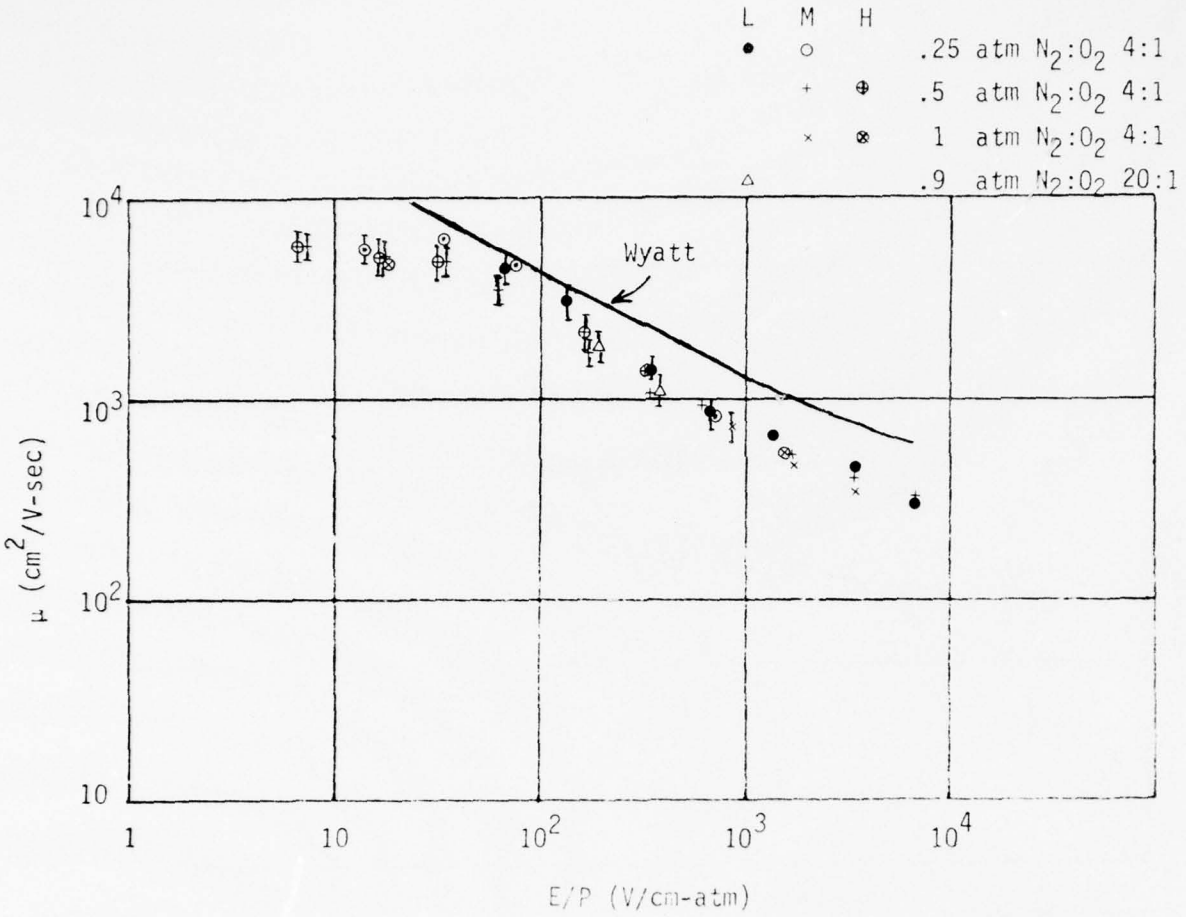

Figure 4.2. μ in dry air.

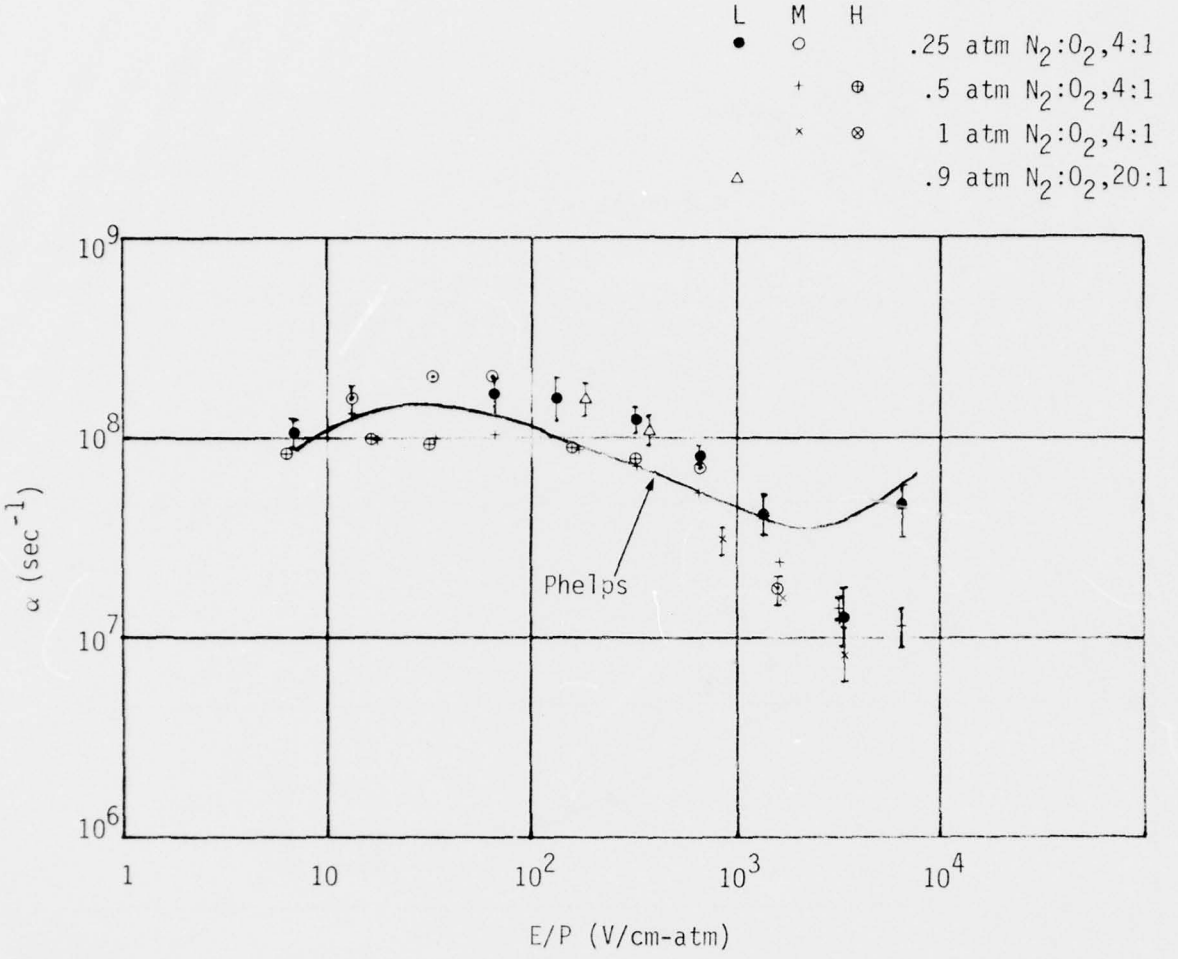

Figure 4.3. α in dry air.

attachment is deeper and occurs at higher E/P than indicated by the Longley and Longmire extrapolation. The expected turnover at low fields is shallower than predicted. The data are consistent with a constant value of

$$\alpha = (10^8 \pm 10\%)\ \text{sec}^{-1}$$

for E/P = 7 to 170 V/cm-atm.

The two data for the 0.9 atm 20:1 N_2:O_2 mixtures when compared to 0.5 atm dry air, indicate that the effectiveness of N_2 as a third body is 3.5% as much as O_2 at E_o/P = 200 to 400 V/cm-atm.

Values of (μ/α) were deduced by dividing the separate quantities, when available at lower pressures or high fields. At 1 atm (μ/α) was deduced from the total charge collected by the ion chamber. The resulting values are plotted in Figure 4.4. The excellent agreement between the 0.5 atm and 1 atm data for E/P $\leq$ 1000 V/cm-atm confirms the dominance of three-body attachment. The systematically low value of the 0.25 atm data is a reflection of the same problem noted in the α values.

4.3 Moist Air Data

Most of the moist air data were taken at 0.5 atm to measure μ and α separately. A few data at 1 atm and 2.75% H_2O confirmed the three body dependence ($1/P^3$ scaling for μ/α).

Figures 4.5 through 4.7 display the mobility data, scaled to 1 atm as 1/P, for various compositions of moist air. Figures 4.8 through 4.10 show the corresponding attachment coefficients. Figures 4.11 through 4.13 show the combined terms, μ/α.

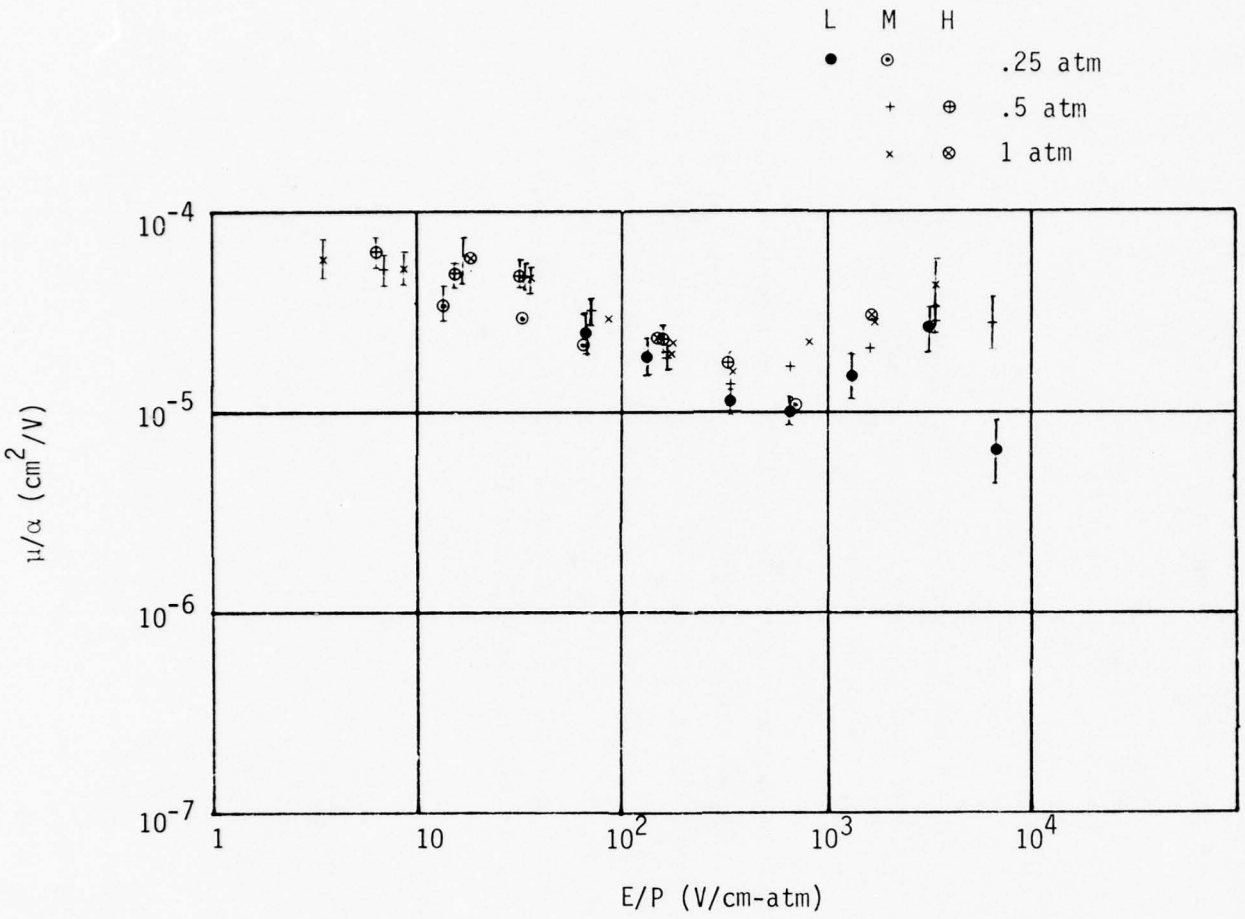

Figure 4.4. μ/α in dry air.

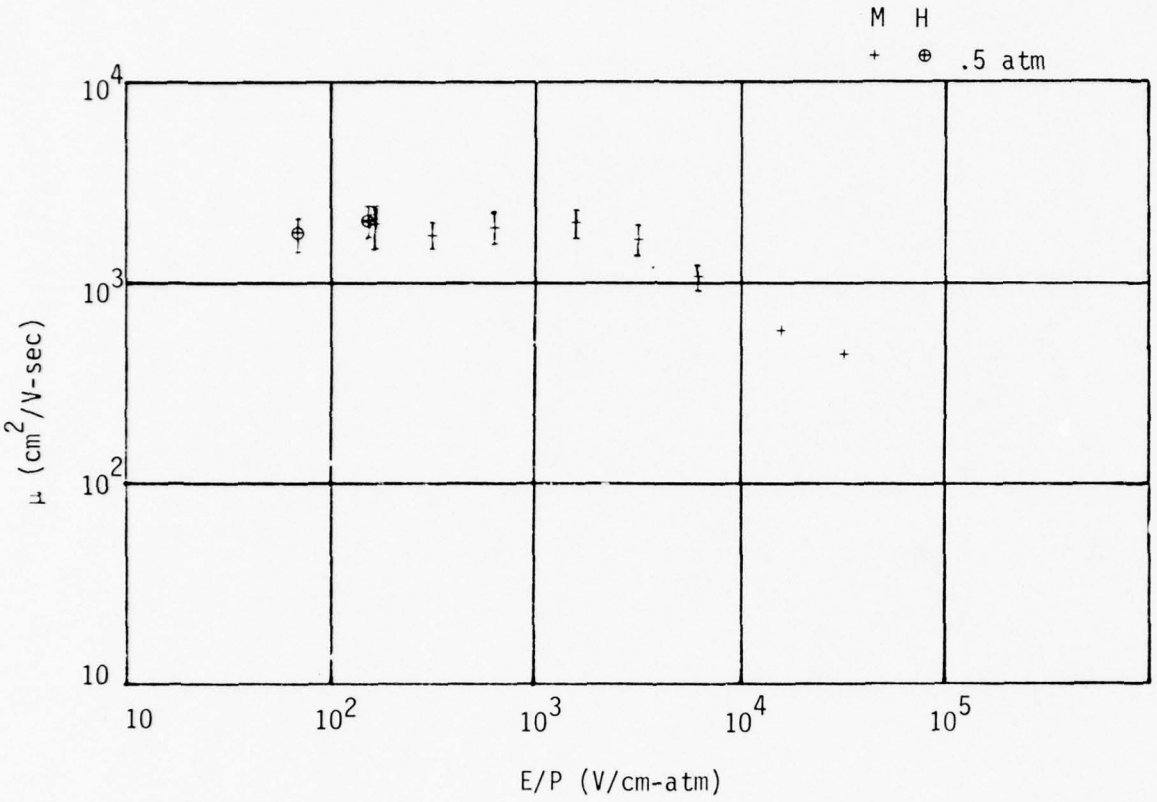

Figure 4.5. μ, air with 2% H_2O.

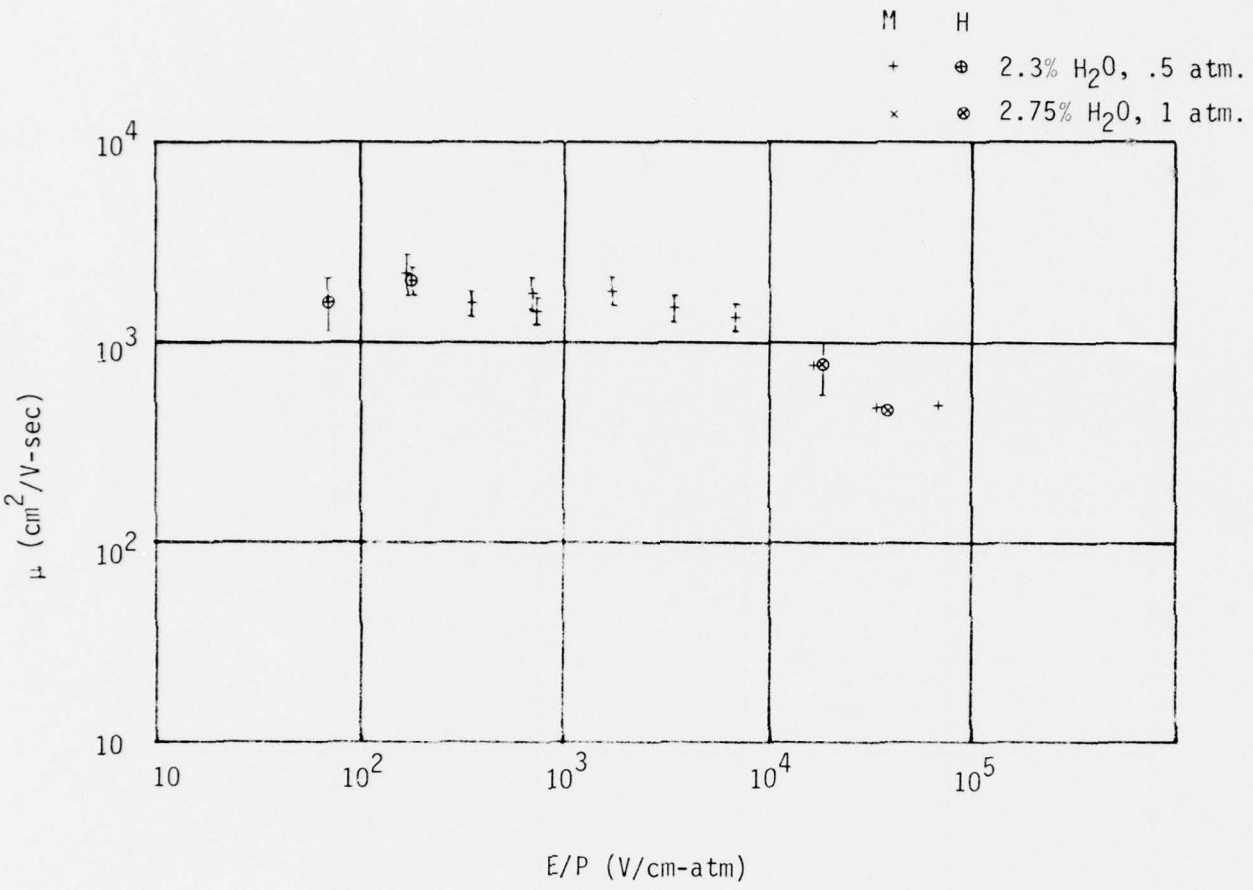

Figure 4.6. μ in air with 2.3% and 2.75% H_2O.

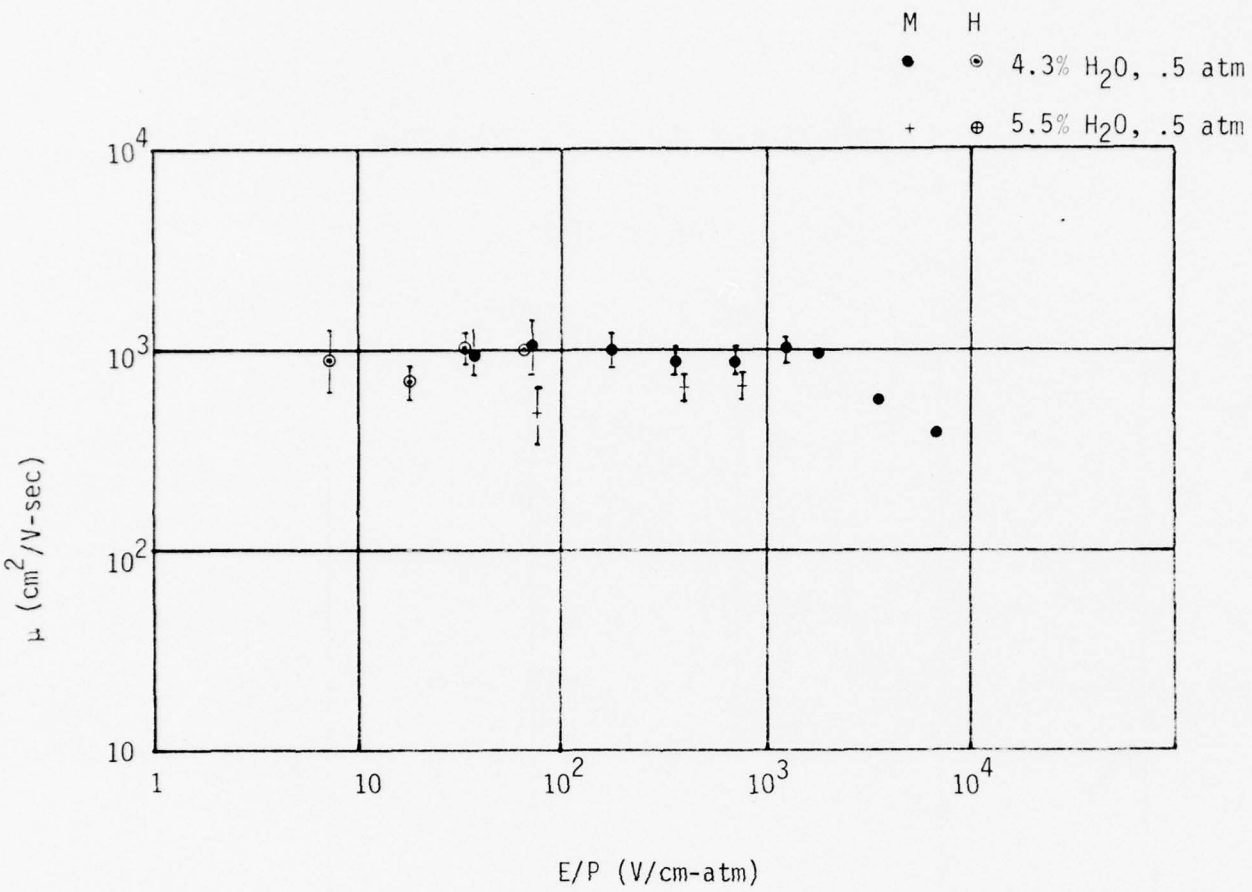

Figure 4.7. μ in air with 4.3% and 5.5% H_2O.

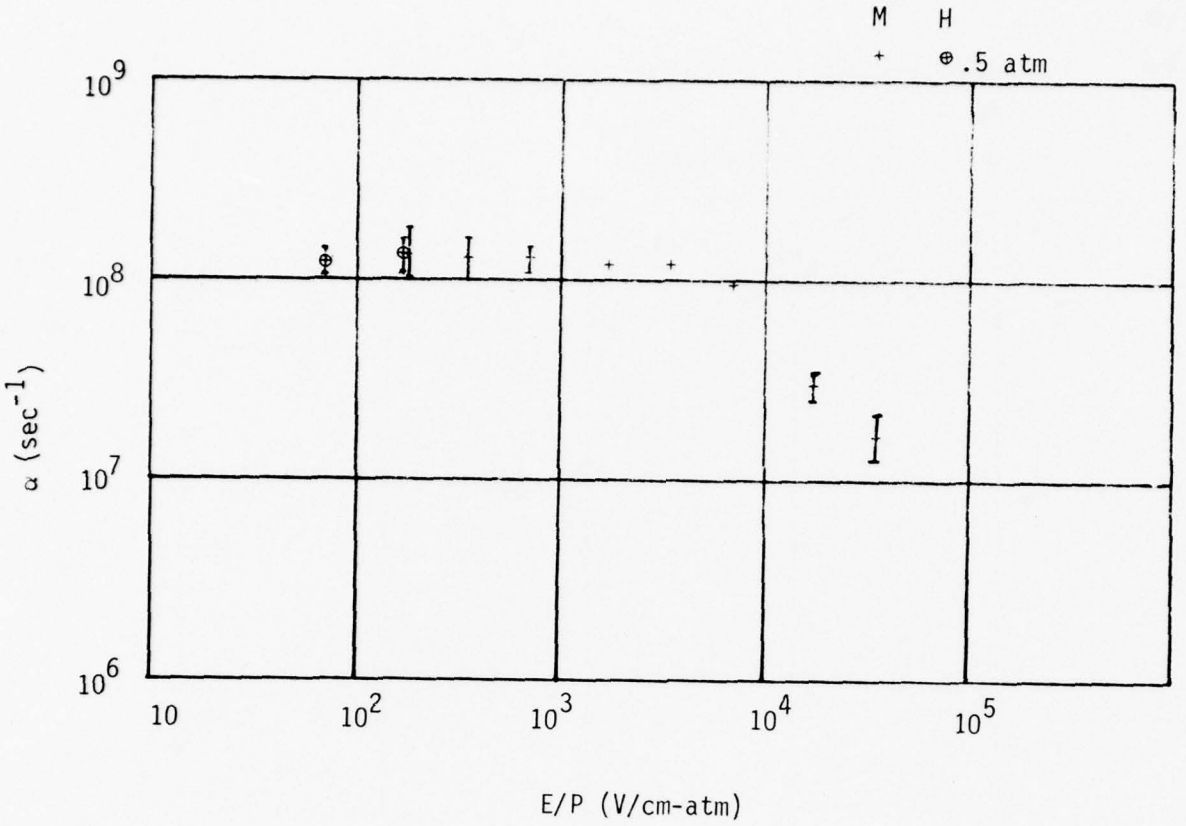

Figure 4.8. α for air with 2% H_2O.

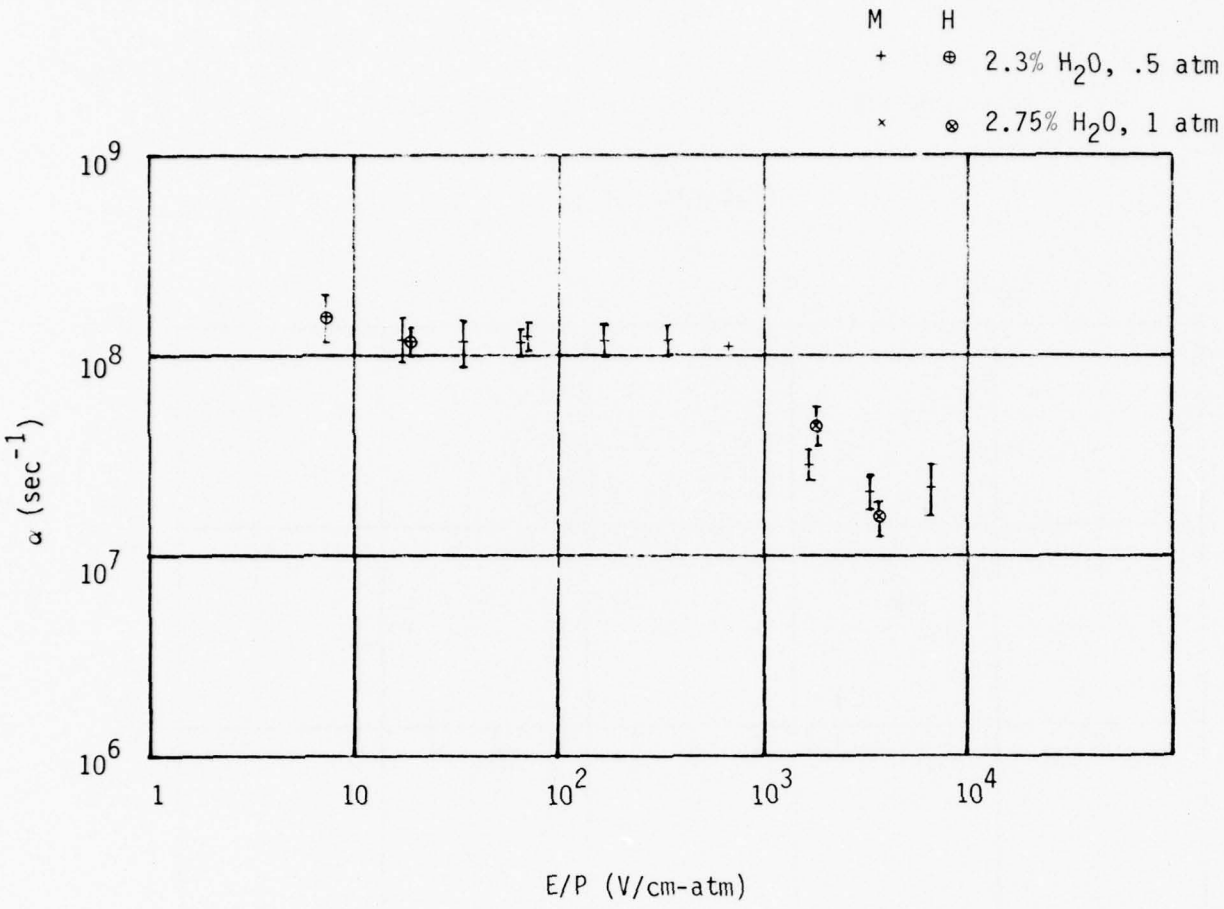

Figure 4.9. α for air with 2.3% and 2.75% H_2O.

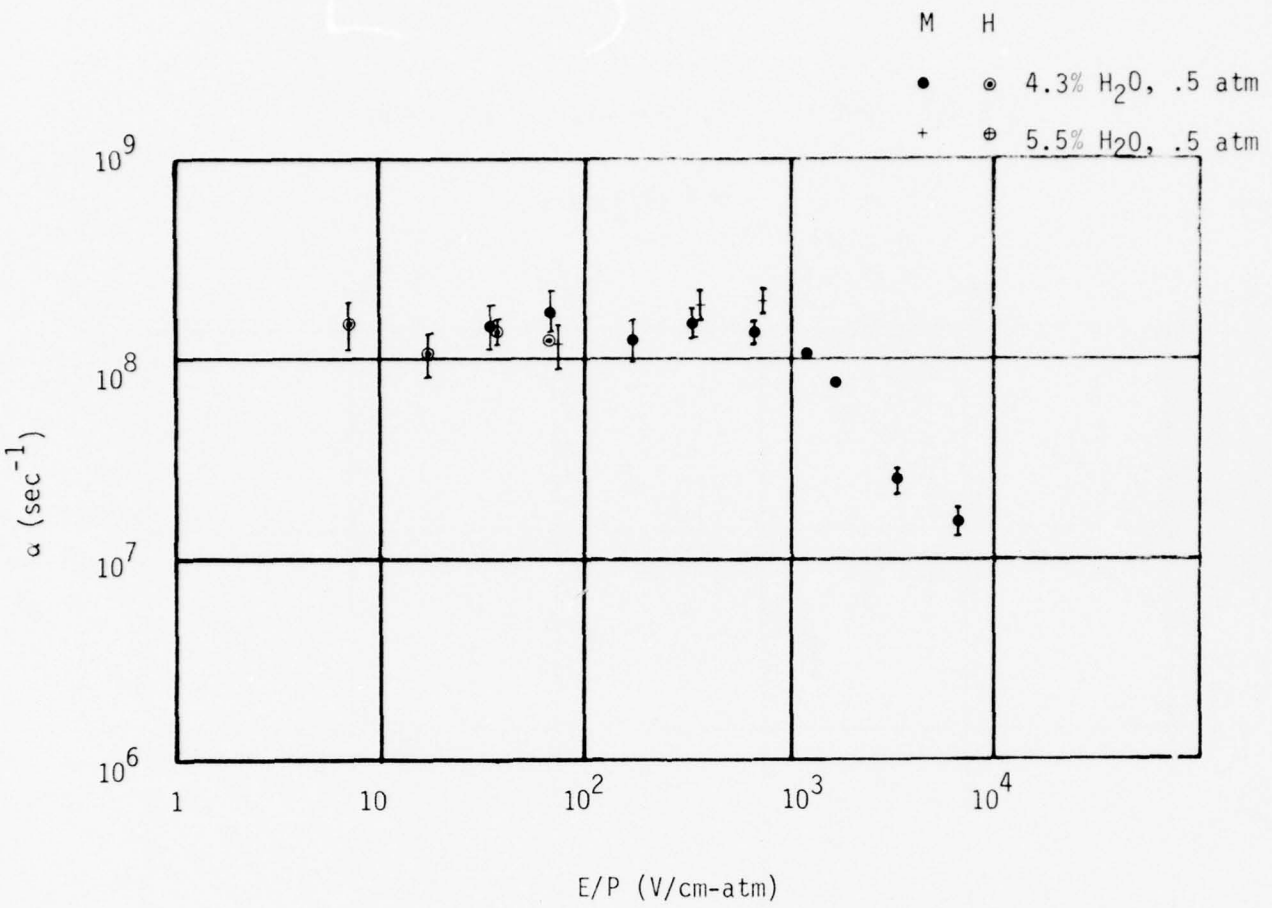

Figure 4.10. α for air with 4.3% and 5.5% H_2O.

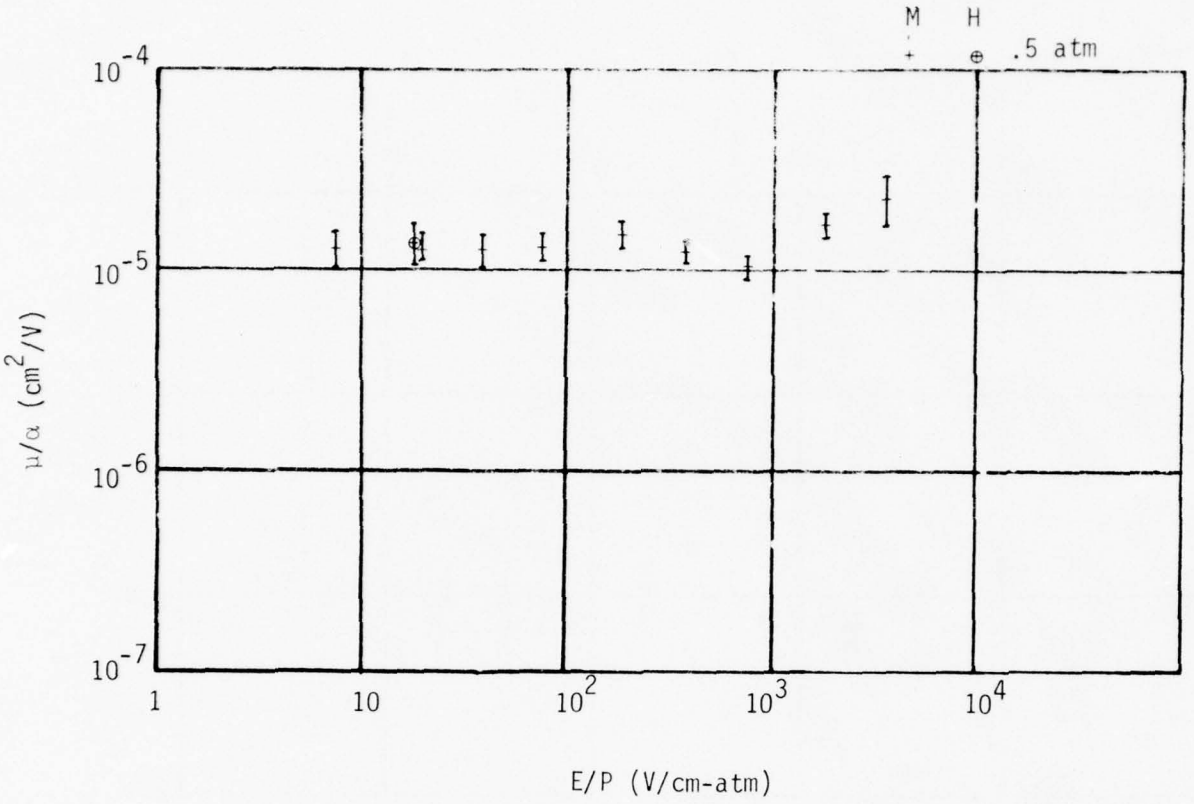

Figure 4.11. μ/α for air with 2% H_2O.

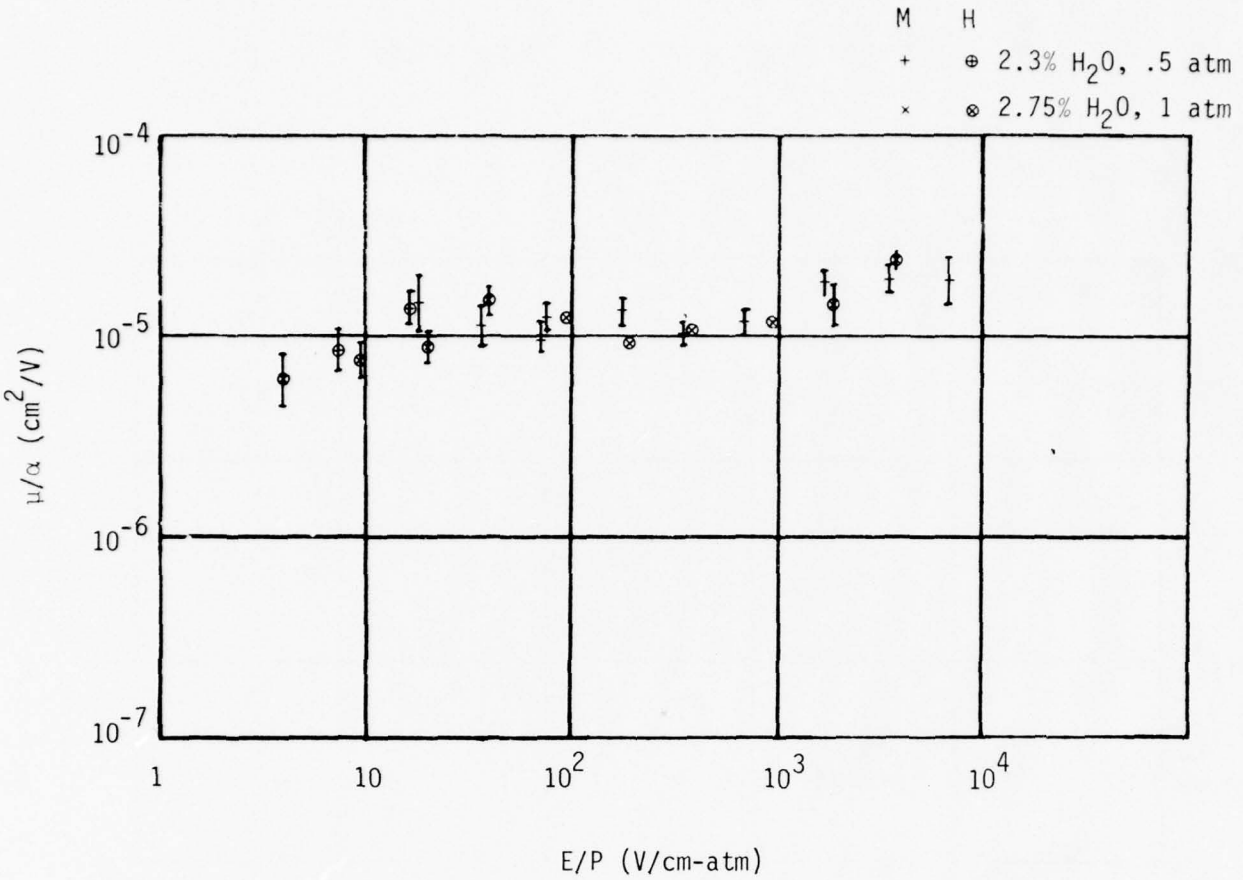

Figure 4.12. μ/α for air with 2.3% and 2.75% H_2O.

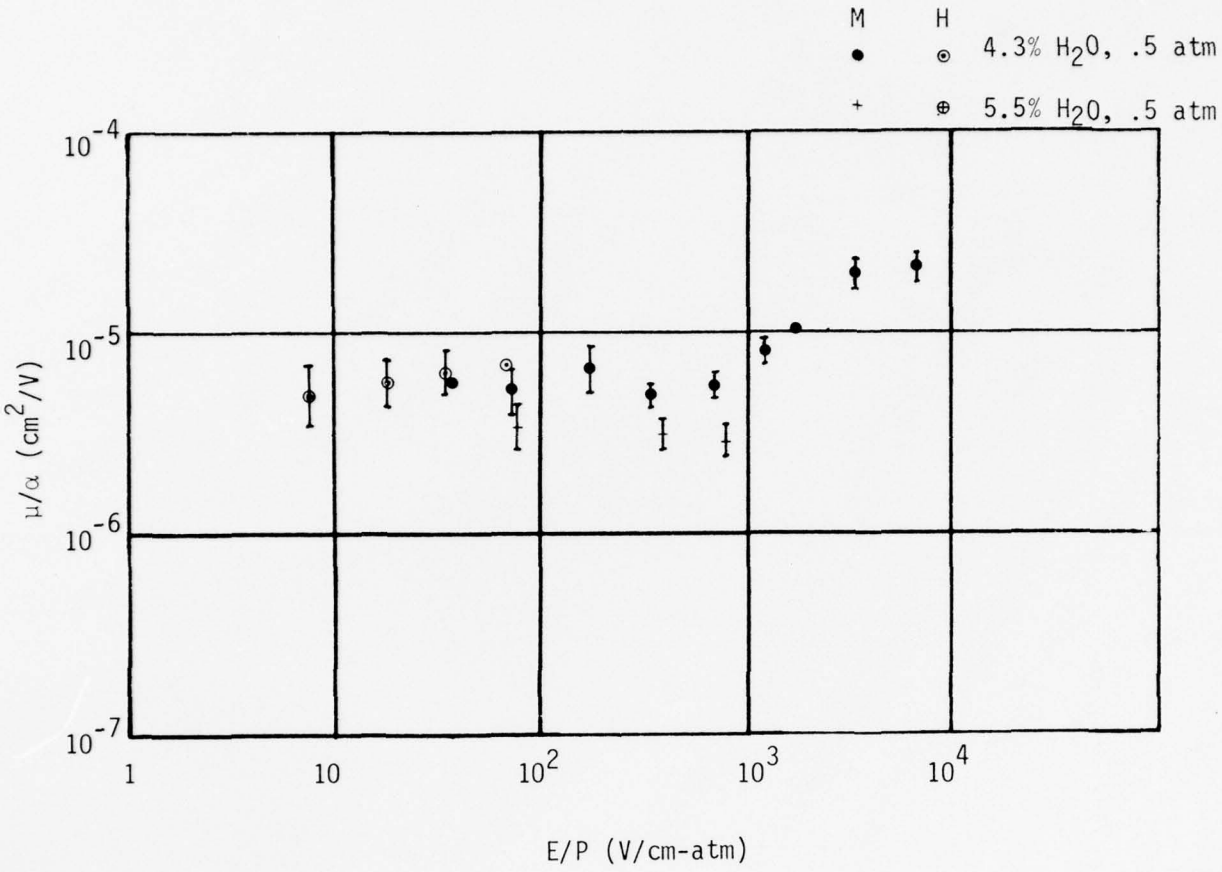

Figure 4.13. μ/α for air with 4.3% and 5.5% H_2O.

Figure 4.12 compares 0.5 atm and 1 atm data at almost equal water vapor concentrations. It is apparent that three-body attachment dominates for $E/P \leq 3800$ V/cm-atm.

SECTION 5

5.0 SUMMARY

Figures 5.1 through 5.3 summarize the data presented in Section 4 by drawing smooth curves through them.

The constant mobility and attachment coefficient extending up to E/P = 200 V/cm-atm for 2% H_2O, and even higher for higher water vapor concentrations testifies to the effectiveness of H_2O molecules in thermalizing electrons. The effectiveness of an H_2O molecule in momentum transfer collisions with electrons can be deduced from Figure 5.4 which presents the plateau value of $(1/\mu)$ vs. H_2O concentration. The decrease in thermal-electron mobility per unit H_2O concentration can be represented as

$$\Delta(1/\mu)/\Delta(\%H_2O) = 2.9\times10^{-4} \text{ V-s/cm}^2.$$

The effectiveness of H_2O as a third body in stabilizing the attachment of electrons to O_2 can be deduced from Figure 5.5, which presents the plateau value of α vs. H_2O concentration.

The net value of α can be expressed as:

$$\alpha = K_{O_2\text{-}O_2}(N_{O_2})^2 + K_{O_2\text{-}H_2O}(N_{O_2})\ (N_{H_2O}).$$

From Figure 5.5,

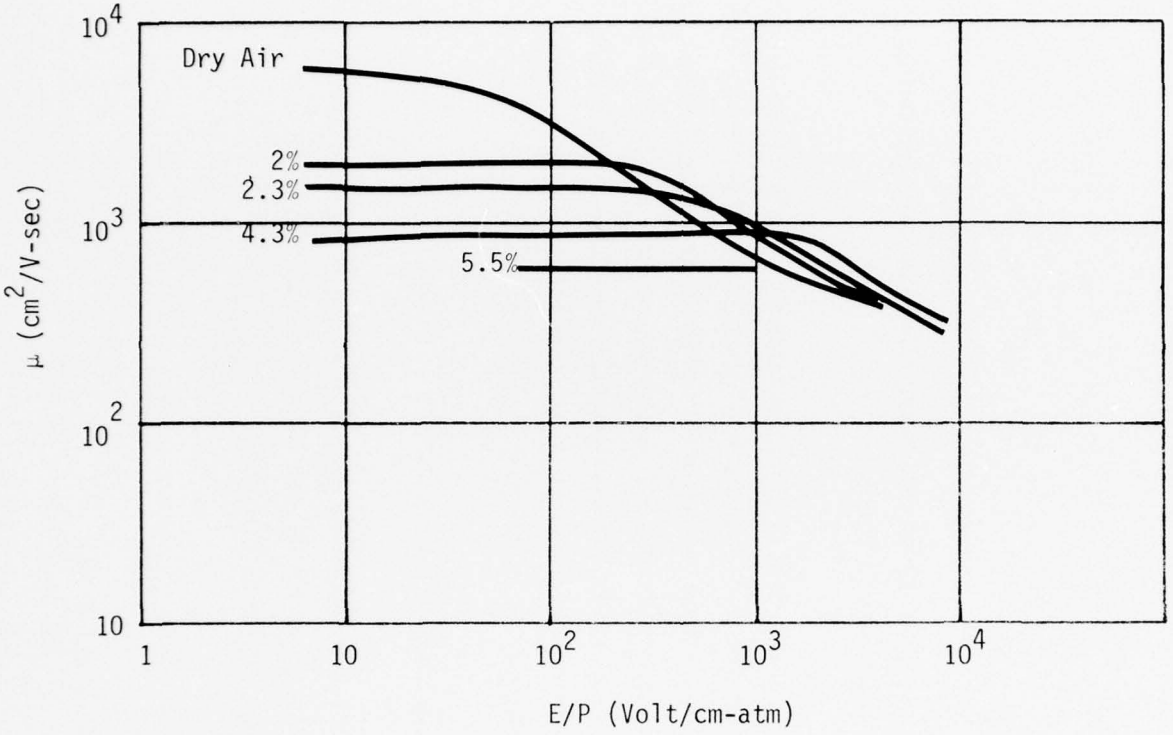

Figure 5.1. μ summary.

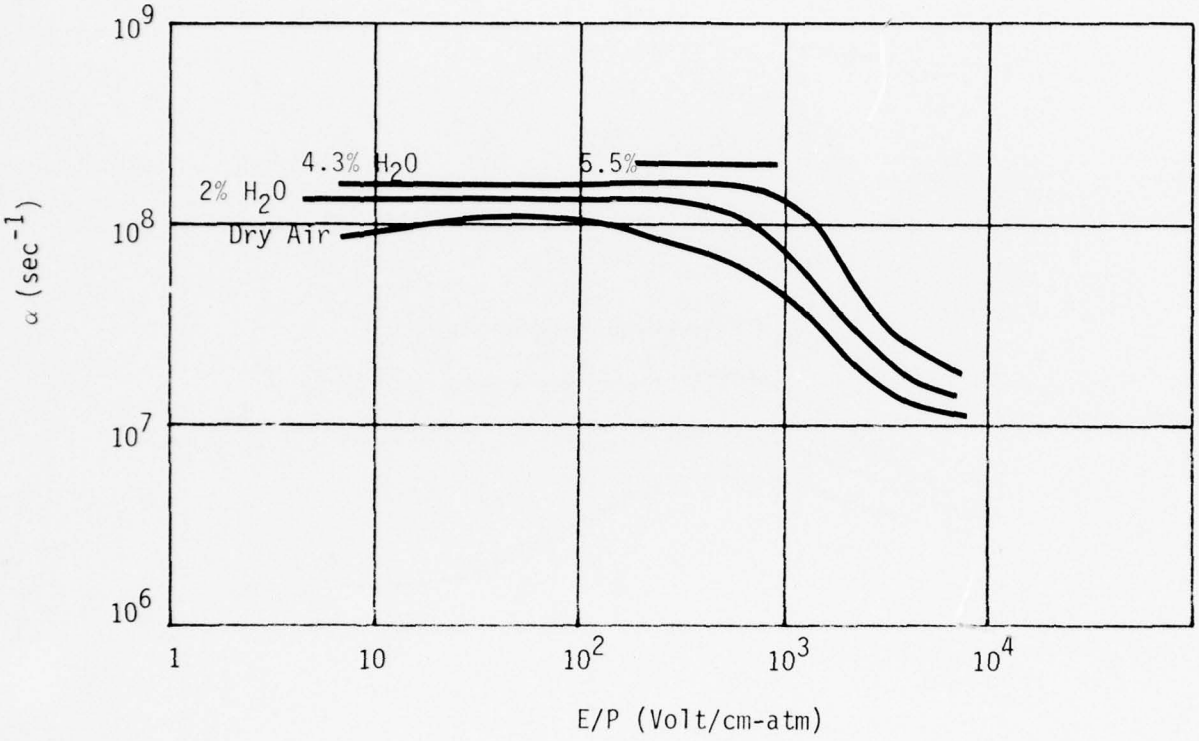

Figure 5.2. α summary.

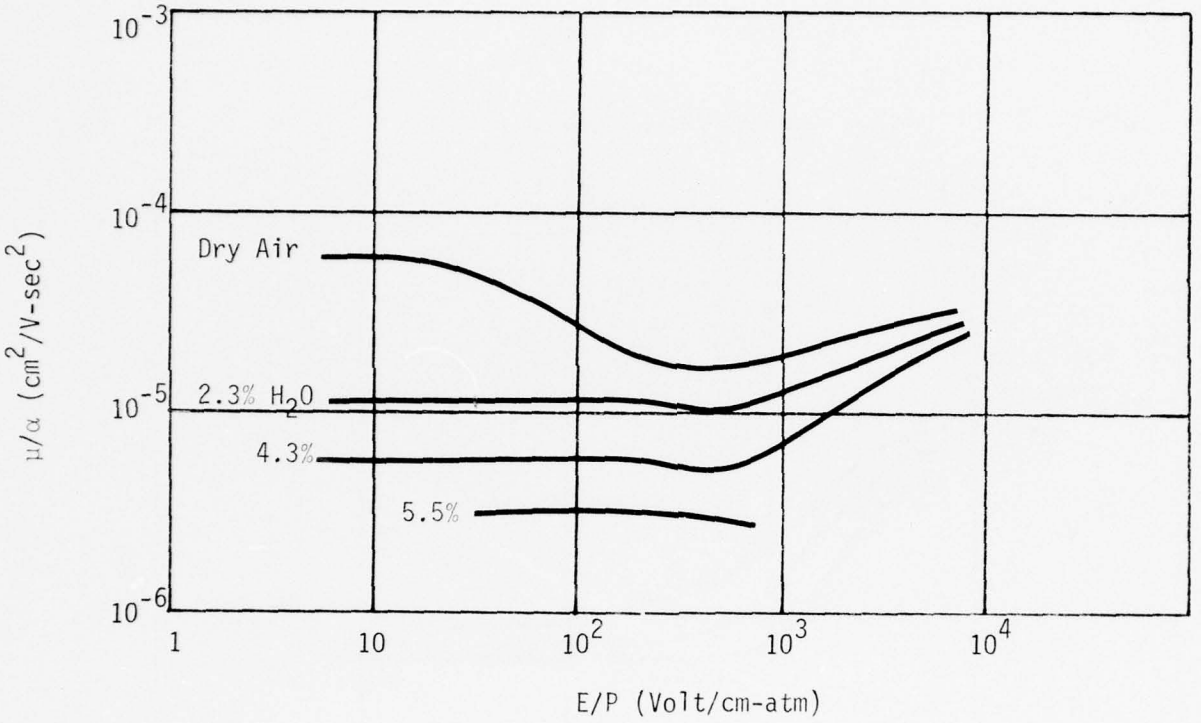

Figure 5.3. μ/α Summary.

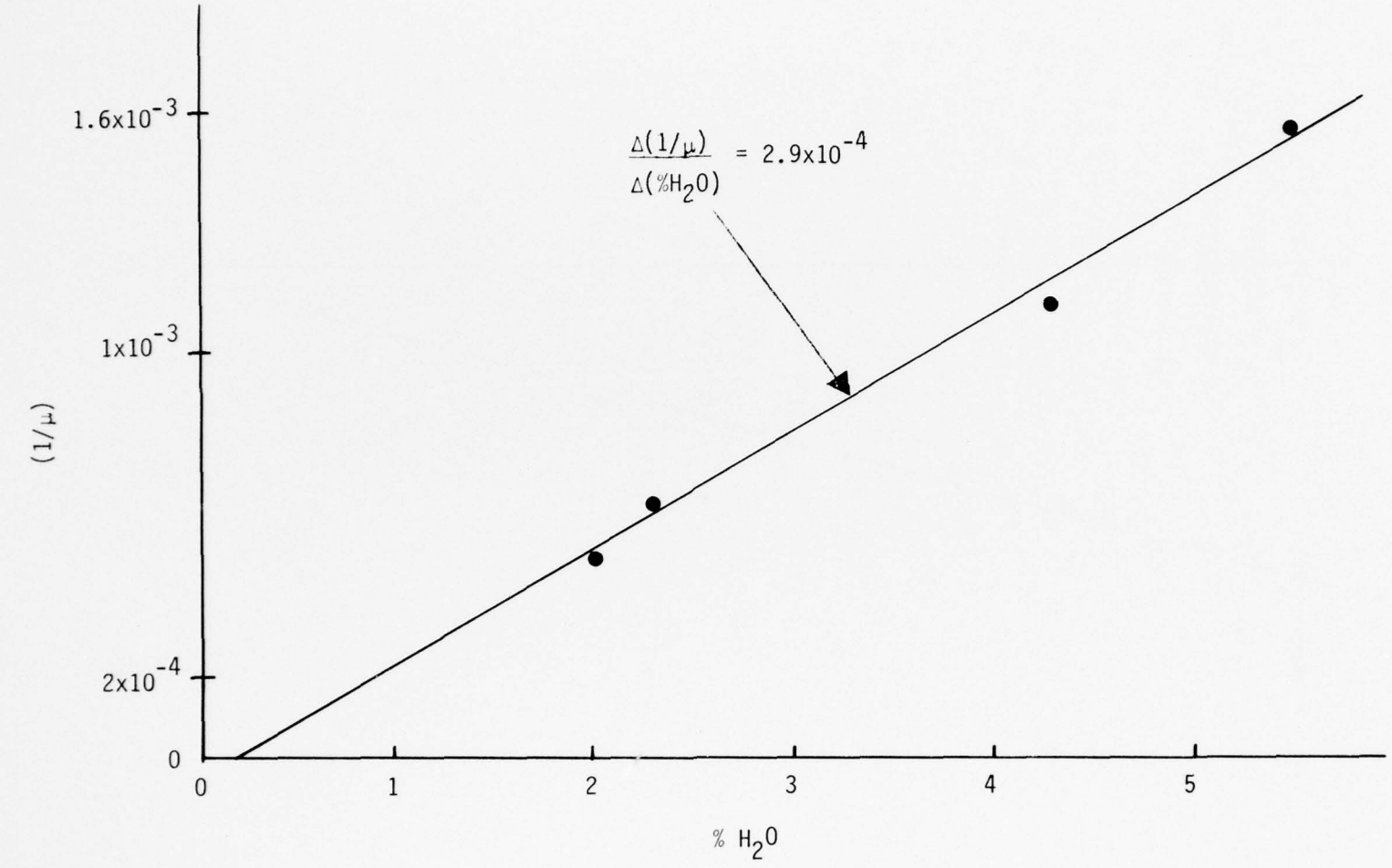

Figure 5.4. Effect of H_2O on mobility of thermal electrons.

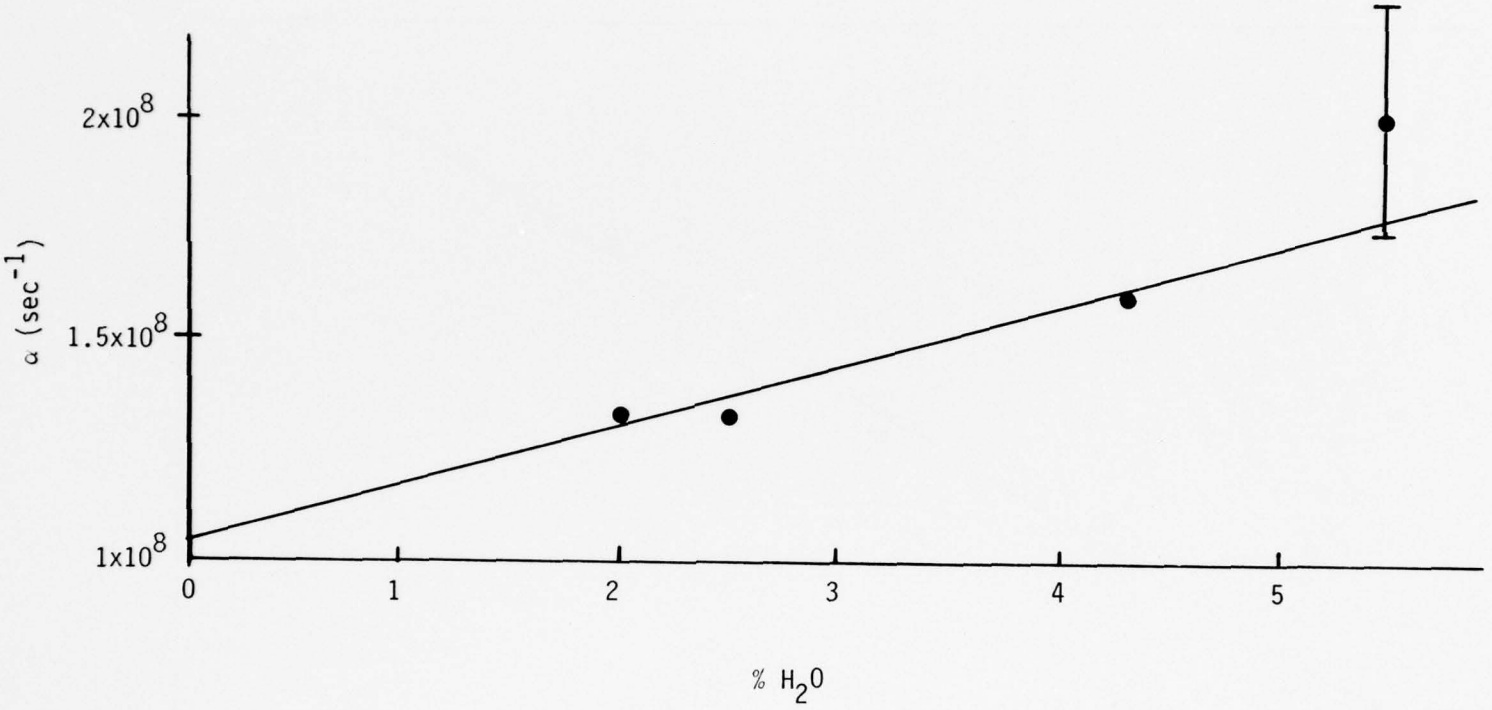

Figure 5.5. Effect of H_2O on α.

$$K_{O_2\text{-}H_2O} = 1.2\text{x}10^{-29} \text{ cm}^6/\text{sec},$$

$$K_{O_2\text{-}O_2} = 3.8\text{x}10^{-30} \text{ cm}^6/\text{sec}.$$

Note that the large uncertainty in the 5.5% data is the result of the few data and the short decay time. Additional data at lower total gas pressure would significantly improve this determination.

The curves in Figures 5.1 through 5.3 have a relative accuracy of ±10% in the mid range, $300 < E/P < 10{,}000$ V/cm-atm. The relative accuracy increases to ~±25% at the ends: due to small signal at low E_o/P, due to sweep-out at high E_o/P. There may be a systematic error of up to -20% in μ and μ/α due to the calibration of the ion pair generation rate. More analysis is required to reduce this uncertainty. At present the possible explanation for the anomalously large values (x1.6) of α in dry air at 0.25 atm has not been checked. Since the 0.5 and 1 atm data agree well and no moist-air data were taken at 0.25 atm it is unlikely that this effect produces an error in the moist-air data, but further effort should be spent to eliminate this uncertainty. If the problem is incomplete thermalization in dry air at 0.5 and 1 atm, it will be absent in moist air due to the high thermalization effectiveness of H_2O.

Additional efforts in the following areas would add confidence in the data and reduce the uncertainty estimates:

1) experiments on H_2O absorption and desorption in the ion chamber to confirm the apparently anomalous 2% H_2O analysis,

2) detailed curve matching to improve the first-order correction for sweep-out applied to these data,

3) detailed curve matching to the He ion chamber data to check calibration,

4) further analysis and possibly HIFX experiments to explain the apparently anomalous 0.25 atm dry-air data,

5) additional measurements at high H_2O concentrations,

and 6) measurements on 0.5 and 1 atm moist air at high fields to detect the onset of two-body attachment.

SECTION 6

6.0 ACKNOWLEDGEMENTS

The authors gratefully acknowledge the considerable contributions of the following persons:

W. N. (Johnny) Johnston (MRC), Leady Ambrose (HLD), Denny Scharf (HDO) who assisted in the construction of experimental equipment and the conduct of the experiment.

Hank Logan and Jim Partridge supported the data processing.

Mr. Joe Silverstein andcrew of the HDL HIFX facility operated the flash X-ray machine, and furnished valuable instrumentation.

Bill Crevier assisted with experiment planning, pretest predictions, and consultation during the experiment and data analysis.

Conrad Longmire established the importance of these measurements.

REFERENCES

1. Longley, H.J. and C.L. Longmire, "Electron Mobility and Attachment Rate in Moist Air", MRC-N-222. Mission Research Corp., December 1975.

2. Crevier, W.F., C.L. Longmire, G. Merkel and D.J. Spohn, "Air Chemistry and Boundary Layer Studies with AURORA", IEEE Trans. Nucl. Sci., NS-24, No. 6, December, 1977.

3. Huxley, L.G. and R.W. Crompton, The Diffusion and Drift of Electrons in Gasses, John Wiley and Sons, 634, 1974.

4. Wyatt, W.F., "Computed Electron Drift Velocity in Moist Air", U.S. Army Engineer Research and Development Laboratories, Report 1890, March 1969.

DISTRIBUTION LIST

DEPARTMENT OF DEFENSE

Armed Forces Radiobiology Research Institute
Defense Nuclear Agency
ATTN: ADLB

Assistant to the Secretary of Defense
Atomic Energy
ATTN: Executive Assistant

Defense Advanced Rsch. Proj. Agency
ATTN: TIO

Defense Documentation Center
12 cy ATTN: DD

Defense Intelligence Agency
ATTN: DB-4C, E. O'Farrell
ATTN: RDS-3A

Defense Nuclear Agency
ATTN: STVL
6 cy ATTN: RAEV
ATTN: RATN
ATTN: DDST
4 cy ATTN: TITL

Field Command
Defense Nuclear Agency
ATTN: FCPR
ATTN: FCLMC

Field Command
Defense Nuclear Agency
Livermore Division
ATTN: FCPRL

Joint Chiefs of Staff
ATTN: J-3

Under Secy. of Def. for Rsch. & Engrg.
Department of Defense
ATTN: Strategic & Space Systems (OS)

DEPARTMENT OF THE ARMY

Deputy Chief of Staff for Rsch. Dev. & Acq.
Department of the Army
ATTN: DAMA-CSS-N, N. Barron

Electronics Tech. & Devices Lab.
U.S. Army Electronics R&D Command
ATTN: DELCS-K, A. Cohen
ATTN: DRDCO-COM-ME, G. Gaule
ATTN: DELET-IR, E. Hunter
ATTN: DELSD-L, W. Werk

Harry Diamond Laboratories
Department of the Army
ATTN: DELHD-N-TL
ATTN: DELHD-N-RBA
ATTN: DELHD-N-P
ATTN: DELHD-N-EM-C
ATTN: DELHD-N-TD
ATTN: DELHD-N-RCC
ATTN: DELHD-N-EMA
ATTN: DELHD-N-EME
ATTN: DELHD-N-RB

DEPARTMENT OF THE ARMY (Continued)

Harry Diamond Laboratories
Department of the Army
ATTN: DELHD-N-EMB
ATTN: DELHD-N-EME
ATTN: DELHD-N-TF
ATTN: DELHD-N-EMD

Multi Service Communications Systems
Department of the Army
ATTN: DRCPM-MSCS-APB, M. Francis

U.S. Army Electronics Rsch. & Dev. Command
ATTN: DRDCO-SEI
ATTN: DRCPM-ATC

U.S. Army Intel. Threat Analysis Detachment
ATTN: Admin. Officer

U.S. Army Test and Evaluation Cmd.
ATTN: DRSTE-FA
ATTN: DRSTE-EL

U.S. Army Training and Doctrine Comd.
ATTN: ATORI-OP-SW

DEPARTMENT OF THE NAVY

Naval Air Systems Command
ATTN: AIR 350F

Naval Electronic Systems Command
ATTN: PME 117-21

Naval Intelligence Support Ctr.
ATTN: Code 41

Naval Ocean Systems Center
ATTN: Code 8123, S. Lichtman

Naval Postgraduate School
ATTN: Code 1424

Naval Research Laboratory
ATTN: Code 1434, E. Brancato
ATTN: Code 2627, D. Folen
ATTN: Code 6624

Naval Surface Weapons Center
ATTN: Code R43, L. Libelo
ATTN: Code F32, E. Rathbun
ATTN: Code F30

Naval Surface Weapons Center
Dahlgren Laboratory
ATTN: Code DF-56

DEPARTMENT OF THE AIR FORCE

Aeronautical Systems Division, AFSC
ATTN: ASD/ENESS, P. Marth
ATTN: ASD/YYEF
ATTN: ASD/ENFTV

Air Force Flight Dynamics Laboratory
ATTN: J. Corbin

DEPARTMENT OF THE AIR FORCE (Continued)

Air Force Weapons Laboratory
ATTN: ELXT
ATTN: SUL
ATTN: ELA, J. Castillo
ATTN: CA
ATTN: ELT, W. Page
ATTN: NT
ATTN: EL, C. Baum
ATTN: NXS
ATTN: NTN
ATTN: ELP

Air Logistics Command
ATTN: OO-ALC/MM, R. Blackburn

Air University Library
Department of the Air Force
ATTN: AUL-LSE-70-250

Electronic Systems Division, AFSC
ATTN: YSEA

Foreign Technology Division, AFSC
ATTN: NIIS Library
ATTN: TQTD, B. Ballard

Rome Air Development Center, TSLD
ATTN: TSLD

Space & Missile Systems Organization
Air Force Systems Command
ATTN: MNNH, M. Baran

Space & Missile Systems Organization
Air Force Systems Command
ATTN: SKF

Strategic Air Command
Department of the Air Force
ATTN: NRI, G. Matzke
ATTN: XPFS, B. Stephan
ATTN: DEL
ATTN: NRI-STINFO Library

OTHER GOVERNMENT AGENCY

Central Intelligence Agency
ATTN: RD/SI, Rm. 5G48, Hq. Bldg.

DEPARTMENT OF ENERGY CONTRACTORS

Lawrence Livermore Laboratory
University of California
ATTN: L-96, T. Donich (Class L-94)
ATTN: Technical Information Dept., Library
ATTN: L-10, H. Kruger (Class L-94)
ATTN: L-156, H. Cabayan

Los Alamos Scientific Laboratory
ATTN: C. Benton
ATTN: B. Noel

Sandia Laboratories
ATTN: E. Hartman
ATTN: R. Parker

DEPARTMENT OF DEFENSE CONTRACTORS

BDM Corp.
ATTN: Corporate Library

BDM Corp.
ATTN: Library
ATTN: J. Schwarz

Bendix Corp.
Research Laboratories Division
ATTN: M. Frank

Dikewood Industries, Inc.
ATTN: L. Davis
ATTN: Technical Library

EG&G Washington Analytical Services Center, Inc.
ATTN: C. Giles

Electro-Magnetic Applications, Inc.
ATTN: D. Merewether

General Dynamics Corp.
Electronics Division
ATTN: Research. Library

General Dynamics Corp.
Inter-Division Research Library
ATTN: Research Library

General Electric Co.
Space Division
ATTN: J. Andrews

General Electric Co.
ATTN: Technical Library

General Electric Company-TEMPO
Center for Advanced Studies
ATTN: DASIAC
ATTN: R. Rutherford
ATTN: W. McNamara

General Electric Company-TEMPO
Alexandria Office
ATTN: DASIAC

General Research Corp.
Santa Barbara Division
3 cy ATTN: Technical Information Office

Georgia Institute Of Technology
Georgia Tech. Research Institute
ATTN: R. Curry

Georgia Institute of Technology
Office of Contract Administration
ATTN: H. Denny

GTE Sylvania, Inc.
Electronics Systems Grp.-Eastern Div.
ATTN: L. Blaisdell
ATTN: C. Thornhill

IIT Research Institute
ATTN: J. Bridges
ATTN: I. Mindel

DEPARTMENT OF DEFENSE CONTRACTORS (Continued)

Institute for Defense Analyses
ATTN: Tech. Info. Services

Ion Physics Corp.
ATTN: R. Evans

IRT Corp.
ATTN: D. Swift

JAYCOR
Santa Barbara Facility
ATTN: W. Radasky

JAYCOR
ATTN: E. Wenaas
ATTN: R. Stahl

JAYCOR
ATTN: Library

Johns Hopkins University
Applied Physics Lab.
ATTN: P. Partridge

Kaman Sciences Corp.
ATTN: W. Ware
ATTN: A. Bridges
ATTN: W. Rich
ATTN: F. Shelton
ATTN: J. Lubell
ATTN: W. Stark

Lutech, Inc.
ATTN: F. Tesche

Maxwell Labs., Inc.
ATTN: W. Travelpiece

Mission Research Corp.
ATTN: EMP Group
ATTN: W. Hart
ATTN: C. Longmire
ATTN: M. Price
ATTN: V. van Lint
5 cy ATTN: Document Control

Mission Research Corp.
ATTN: A. Chodorow
ATTN: L. McCormick

Physics International Co.
ATTN: Document Control

DEPARTMENT OF DEFENSE CONTRACTORS (Continued)

R & D Associates
ATTN: C. Mo
ATTN: R. Schaefer
ATTN: S. Rogers
ATTN: C. MacDonald
ATTN: Document Control

R & D Associates
ATTN: J. Bombardt

Rand Corp.
ATTN: LIB-D

Rockwell International Corp.
ATTN: D/243-068, 031-CA31
ATTN: J. Monroe
ATTN: V. Michel
ATTN: N. Rudie

Rockwell International Corp.
ATTN: B-1 Div. TIC (BA0B)

Rockwell International Corp.
ATTN: F. Shaw

Science Applications, Inc.
ATTN: R. Parkinson

Science Applications, Inc.
Huntsville Division
ATTN: N. Byrn

Science Applications, Inc.
ATTN: W. Chadsey

Sidney Frankel & Associates
ATTN: S. Frankel

Spire Corp.
ATTN: R. Little

SRI International
ATTN: A. Whitson

TRW Defense & Space Sys. Group
ATTN: L. Magnolia
ATTN: O. Adams
ATTN: R. Plebuch
ATTN: H. Holloway

TRW Systems and Energy
ATTN: D. Pugsley